INL/EXT-18-51053-Revision-0

# Bison Fuel Performance Modeling on RIA in a PWR

Wenfeng Liu, Anh Mai, John Alvis, Joe Rashid, Charles P Folsom

July 2018


The INL is a U.S. Department of Energy National Laboratory
operated by Battelle Energy Alliance

INL/EXT-18-51053-Revision-0

# Bison Fuel Performance Modeling on RIA in a PWR

**Wenfeng Liu, Anh Mai, John Alvis, Joe Rashid, Charles P Folsom**

**July 2018**

**Idaho National Laboratory**
**Idaho Falls, Idaho 83415**

**http://www.inl.gov**

**Prepared for the**
**U.S. Department of Energy**

**Under DOE Idaho Operations Office**
**Contract DE-AC07-05ID14517**

CASL-U-2018-1656-000

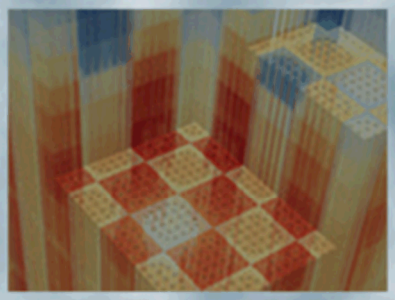

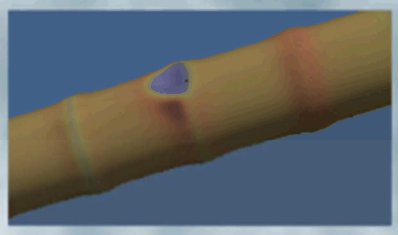

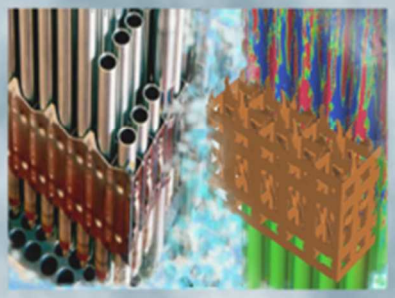

# Bison Fuel Performance Modeling on RIA in a PWR


Wenfeng Liu[1]
Anh Mai[1]
John Alvis[1]
Joe Rashid[1]

Charles Folsom[2]

[1]Structural Integrity Associates, Inc.
[2]Idaho National Laboratory


**Date July 30, 2018**

U.S. DEPARTMENT OF ENERGY | Nuclear Energy

**Please complete sections appropriate for this record.**

**REVISION LOG**

| Revision | Date | Affected Pages | Revision Description |
|---|---|---|---|
| 0 | | All | Initial Release |
| | | | |
| | | | |
| | | | |

**Document pages that are:**

Export Controlled _____NONE_____

IP/Proprietary/NDA Controlled_____NONE_____

Sensitive Controlled_____NONE_____



**Requested Distribution:**

To: FMC FA Lead

Copy: CASL PM

# EXECUTIVE SUMMARY

This report is prepared to fulfill a Level 2 milestone for CASL on "deliver and document RIA fuel performance modeling using Bison fuel performance code." The work performed is focused on modeling the full length commercial fuel rod response under a design basis Reactivity Initiated Accident (RIA), in particular, a hypothetical Control Rod Ejection Accident (CREA) in a Pressurized Water Reactor (PWR). Fuel rods with different burnups, 0 (fresh fuel), 20, 40, and 60 GWd/tU have been modeled with a reactivity worth insertion of $1.24 at Hot Zero Power (HZP) condition. Bison failure modeling method, and a brief summary of validations on selected RIA cases from CABRI and NSRR testing facilities are also described.

The work performed has demonstrated the successful application of Bison code in the modeling of thermal and mechanical responses in RIAs for PWRs. In particular, Bison code has a more mature capability in the modeling of the frictional contact between pellet and cladding of the high burnup fuels, which is critical for modeling the Pellet Clad Mechanical Interaction (PCMI).

The modeling of RIA using Bison code shows fuels in PWR environment could have different responses than in the simulated RIA tests, and results indicate that a transition from PCMI to Departure from Nucleate Boiling (DNB) could happen at relatively lower enthalpies: a better heat transfer from the fuel to coolant could increase cladding temperature and ductility, but at the same time also reduces the margin to DNB, which could cause high temperature oxidation and ballooning type of failures. The precise determination of the transition into DNB may rely on a more accurate input of the power histories in the simulated RIAs from VERA, the core simulator of CASL. The limiting conditions in PWRs could be quite different than those tests with non-typical testing conditions, and the improvement of the modeling of thermal responses, such as, clad coolant heat transfer, gap heat transfer, clad thermal inertia, and radial power profiles could be important considerations of the RIAs. In modeling the fuel responses in a fast transient, a number of variables could affect the initial burnup states, and some material models, e.g., fuel mechanical models, fission gas release, and corrosion models, and parameters can affect modeling results as well. Those uncertainties and advanced modeling capabilities need to be investigated in the future study of RIAs.

CONTENTS

EXECUTIVE SUMMARY ..... iv

1. INTRODUCTION ..... 1

2. METHODOLOGY ..... 3
2.1 PCMI Failure Model ..... 3
2.2 High Temperature Failures ..... 5

3. RIA EXPERIMENTS MODELING ..... 7

4. MODELING PWR REA ..... 10
4.1 NEA benchmark case description ..... 10
4.2 Bison Input Models ..... 11
4.3 Initial Burnup Condition ..... 14

5. PWR REA RESULTS ..... 17
5.1 Results for the base case ..... 17
5.2 Fuel thermal and mechanical responses at different burnups ..... 18
5.3 Scaling to high powers ..... 21
5.4 Modeling high temperature failures ..... 24
5.5 Fuel mechanical modeling ..... 25

6. CONCLUSIONS ..... 26

REFERENCES ..... 27

**List of Figures**

Figure 1: RIA power pulse schematic showing the relationship between power, energy deposition, and radial average peak fuel enthalpy ..... 1
Figure 2: Evolution of RIA fuel failure mechanisms as a function of burnup, and impact on key fuel rod characteristics [1] ..... 2
Figure 3: Strain energy density calculated by Bison in comparison to a CSED (as a function of total hydrogen content) failure model; solid symbol represents failure case, and hollow symbol represents non-failure case ..... 5
Figure 4: Comparison between Bison calculated failure enthalpy (determined as the enthalpy at predicted CSED) and measurement for the failure cases ..... 5
Figure 5: Peak cladding temperature measured in NSRR tests at ambient condition [15] ..... 6
Figure 6: Comparison between calculated and measured peak clad elongation for Bison and Falcon 9
Figure 7: Comparison between Bison and Falcon calculations of strain energy density for CABRI and NSRR cases ..... 9
Figure 8: Core map for the simulated control rod ejection accidents at hot zero power condition: a) Case A1, peripheral control assembly is ejected, and b) Case C1, central control assembly is ejected [6] ..... 10
Figure 9: Core relative power for case A1 and case C1 ..... 11
Figure 10: Finite element mesh used for the PWR REA case ..... 12
Figure 11: Power pulse history of case C1 during the RIA (Peak LHGR = 424.35 kW/m) ..... 12
Figure 12: Axial power profiles for the test cases A1 and C1 ..... 12
Figure 13: Bison calculated maximum oxide thickness in comparison to measurement ..... 14
Figure 14: The gap factor (ratio of cold gap size to as-fabricated gap size) for irradiated fuel, determined from code calculation and measurement data [26] ..... 15
Figure 15: Radial burnup profile at different burnups of 20, 40, and 60 GWD/tU ..... 15
Figure 16: Radial power profile at different burnups of 0, 20, 40, and 60 GWD/tU ..... 16
Figure 17: Calculated oxide thickness and hydrogen content in a PWR fuel at different burnup ..... 16
Figure 18: Hydrogen content in test rods in CABRI and NSRR tests at high burnup ..... 17
Figure 19: Comparison between case C1 and A1 on peak fuel radial average enthalpy ..... 18
Figure 20: Fuel centerline, fuel outer surface, clad inner and outer surface temperatures ..... 18
Figure 21: Peak radially averaged fuel enthalpy at different burnups ..... 19
Figure 22: Gap conductance and gap size in simulated RIA at different burnups ..... 19
Figure 23: Fuel centerline and outer surface temperature at different initial burnup during RIA ..... 20
Figure 24: Clad surface temperature at different burnups ..... 20
Figure 25: Clad outer surface hoop and axial stress at different burnups ..... 20
Figure 26: Clad outer surface strain energy density at different burnups ..... 21
Figure 27: Maximum strain energy density at different fuel enthalpies ..... 22
Figure 28: Maximum fuel enthalpy rise for REA at HZP [23] ..... 23
Figure 29: Comparison on the thermal and mechanical responses between 40 GWd/tU and 60 GWd/tU at scaled high power ..... 24
Figure 30: Clad surface SED and temperature under the conditions with DNB using scaled power (peak power x 4) ..... 25
Figure 31: Comparison of fuel enthalpy and clad surface temperature for fresh fuel with different powers ..... 25
Figure 32: Comparison of fuel mechanical models on the fuel radial displacement and strain energy density in clad ..... 26

**List of Tables**

Table 1: Summary of the Bison calculated characteristics for the NSRR cases in comparison with measurements and Falcon calculations [9] ..... 7
Table 2: Summary of the Bison calculated characteristics for the CABRI cases in comparison with measurements and Falcon calculations [8] ..... 8
Table 3: Neutronic characteristics of REA cases ..... 10
Table 4: Design and operation parameters ..... 11
Table 5: Bison input models ..... 13
Table 6: Fuel characteristics at different burnup levels ..... 14
Table 7: Calculated CSED and hydrogen content at different burnup levels: 20, 40, and 60 GWd/tU ..... 17
Table 8: Results of clad mechanical and thermal responses at different peak powers at the burnup of 60 GWd/tU ..... 21
Table 9: Results of fuel enthalpy, clad outer surface SED and temperature at 0.5 sec for the case with 60 GWd/tU ..... 22

# 1. INTRODUCTION

Design basis Reactivity Initiate Accidents (RIAs) could have adverse impacts on the core coolability. This postulated accident results from an inadvertent insertion of reactivity due to the ejection of a control rod assembly in a PWR or the drop of a control blade in a BWR. In the unlikely event that sufficient reactivity is inserted into the reactor core by the ejected/dropped control rod, prompt energy deposition into the fuel can occur, which when sufficiently high can lead to fuel rod failure or, at large energy deposition levels, expulsion of $UO_2$ fragments or molten $UO_2$ material from the fuel rod. The schematic in Figure 1 highlights the relationships between the power pulse, the energy deposition and the radial average fuel enthalpy. The energy deposition represents the integration of the power-time curve and reaches the total energy deposited once the power returns to zero. The radial average fuel enthalpy is calculated based on the $UO_2$ specific heat and the radial temperature profile. A maximum is reached near the late part of the power pulse as heat conduction effects begin to dominate. The relative response of these different parameters depends on the pulse width defined by the Full-Width Half Maximum (FWHM) of the power pulse.

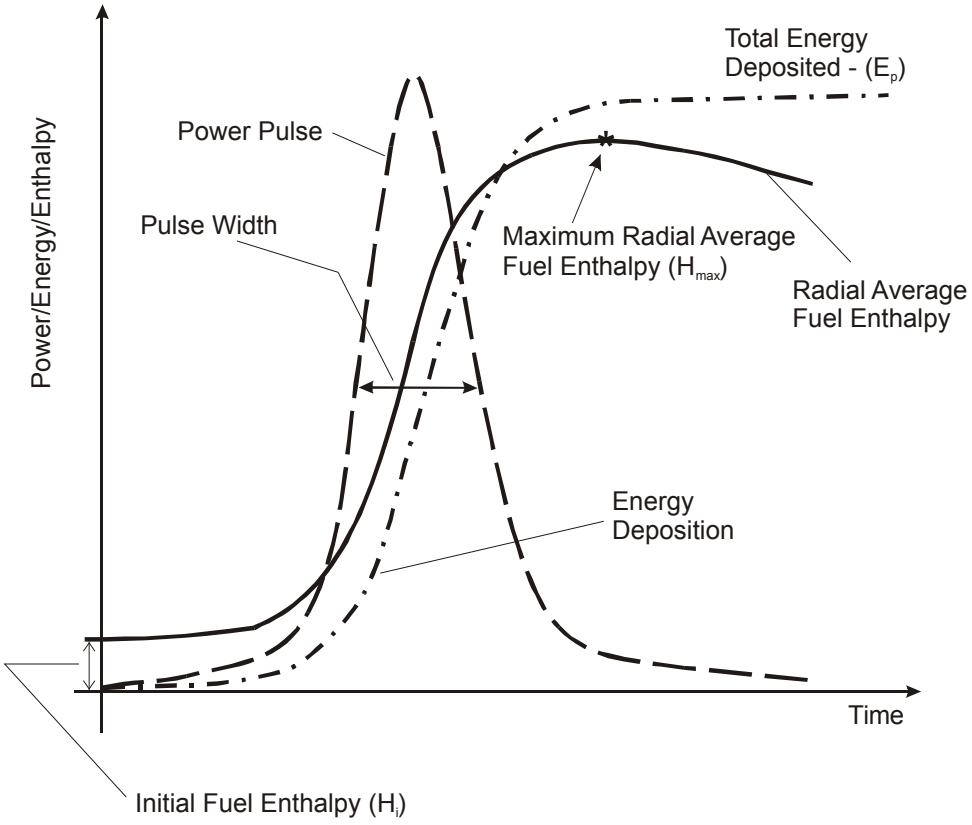


Figure 1: RIA power pulse schematic showing the relationship between power, energy deposition, and radial average peak fuel enthalpy

At higher burnups, the hydride precipitates, as a result of the hydrogen pickup during the cladding water-side corrosion process, significantly reduces the cladding ductility leading to the potential of fuel rod failure from PCMI during a RIA. Additionally, during the transient, depending on energy deposition in the fuel, the cladding outer surface could experience Departure from Nucleate Boiling (DNB). This generally causes a cladding surface temperature excursion, and can have temperatures exceeding 800ºC, depending on the power level (heat flux) and coolant conditions. This could cause cladding temperature to rise and enable clad ballooning and rupture, and/or induce high temperature oxidation and embrittlement. Figure 2 illustrates schematically the failure mechanisms and their dependency on burnups.

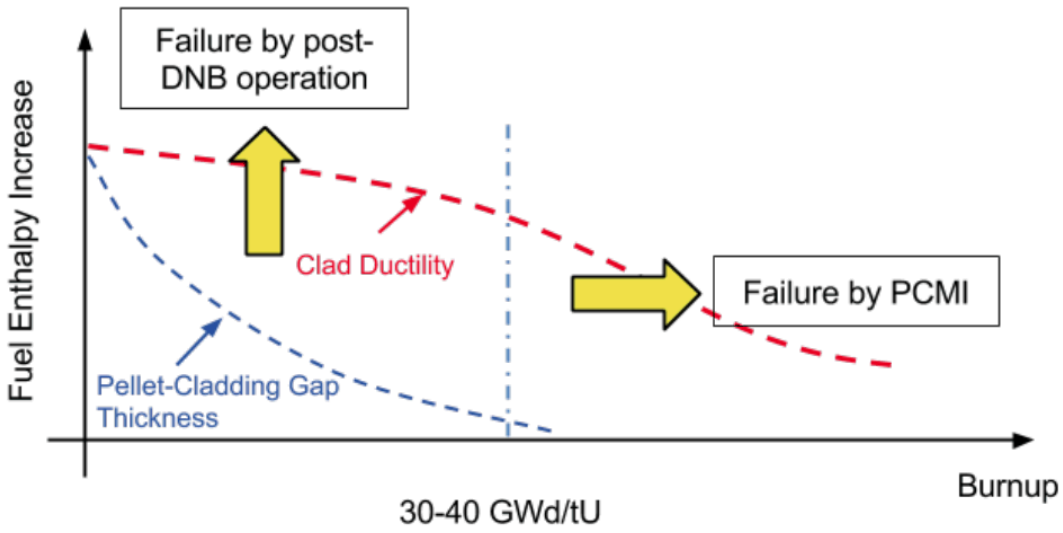


Figure 2: Evolution of RIA fuel failure mechanisms as a function of burnup, and impact on key fuel rod characteristics [1]

The hydride embrittled cladding failure due to PCMI occurs at low energy deposition, as was observed in the NSRR and CABRI test facilities [2-5] and has become a major concern for burnup extension. However, the characteristics in those simulated RIA tests are not representative of the conditions in a commercial reactor; NSRR has a narrow power pulse (~5 ms) and stagnant coolant water with many tests conducted at ambient conditions, and the CABRI sodium loop test cannot simulate the coolant boiling. Therefore, further study on the high burnup fuel under realistic reactor condition is still need. It is hoped that the research program being conducted by the CABRI International Project (CIP) will provide more relevant experimental data. Even so, the information from the test reactor data still must be interpreted to understand the fuel response under RIA in a commercial reactor condition. Fuel performance modeling is a valuable tool to understand these failure mechanisms and to quantify the safety margin.

As part of CASL's research on the modeling and simulations of RIAs, Bison code is used as the tool for the interpretation of test data, and for modeling PWR CREAs. Current work is focused on modeling thermal-mechanical response of full length fuel rod in a design basis control rod ejection accident conditions in PWRs using Bison. The calculated fuel response is compared to the failure conditions determined from simulated RIA tests and model analysis. The fuel rod responses were modeled using power pulse history and axial power profiles generated from the output of a neutronic code, PARCS, in a benchmark problem [6, 7]. PWR fuel rods were modeled by assuming different initial burnup condition for the RIAs. A benchmark case with a peripheral CREA in PWR with an inserted reactivity of $1.24 is selected as the baseline for the study. A simple scaling is applied to the rod average power during RIAs to extend the Bison modeling at different fuel enthalpies to quantify the margin to fuel failures.

Despite those limitations, current results provide more realistic responses in the PWR conditions than in the test reactor conditions. Results have shown differences between the fresh fuel and the high burnup fuel in the calculated thermal-mechanical responses. Differences between PWRs and the test reactor in the modeling of the occurrence of DNB are also noted. The PCMI failure threshold derived from test reactor data is conservative. Recent test data has demonstrated that PCMI failure either from the lower injected enthalpies typical of a PWR event or from ductility recovery in the cladding due to clad temperature increasing with reactor power prevents the occurrence of PCMI failures.

Key input models used for the modeling of RIAs are also documented and discussed for a future reference. Note that, in the RIA, the thermal and mechanical responses are strongly coupled, and

results could be highly dependent on the models and parameters used. Those uncertainties may need to be quantified in the future research. Improvements in the accuracy of modeling the thermal responses and fuel mechanical models would be of interest to the RIA modeling as well.

The report is organized as follows. Section 2 will describe the failure modeling methodology on both PCMI failure and high temperature failures. Section 3 provides a brief update of the experimental validation on the simulated RIA tests using Bison. Note that details on the Bison validation will be provided in a separate milestone report [8]. Section 4 describes the test cases used for the modeling of PWR CREA. Input models and assumptions for the fuel rod conditions at different burnups will be provided as well. Section 5 describes the modeling results including a comparison of the results at different burnups, and an evaluation of both PCMI and high temperature DNBs by scaling the power magnitude, and the effects of initial fuel condition and models on the failure metrics.

# 2. METHODOLOGY

## 2.1 PCMI Failure Model

The potential to have a PCMI type of failure in a hypothetical RIA condition depends on the mechanical load during the RIA and the ductility of the pre-irradiated cladding. The evaluation of RIA test cases uses a Critical Strain Energy Density (CSED) failure modeling approach which consists of: a) The development of a CSED failure model, and b) Bison code validation on the thermo-mechanical modeling of RIA including the validation of modeling PCMI failure.

The model development has been detailed in the Ref. [9]. Closed-end tube burst tests on irradiated cladding tubes at high fluences were selected as the database for the development of the failure model since burst tests, among the mechanical property tests, best represent the biaxial load in a RIA with strong PCMI. CSED as a function of $C_H$ (total hydrogen content), is given in the following formula:

$$\text{CSED} = 31.83\exp(-0.0029C_H) + 4.0 \qquad 1)$$

The hydrogen content in the test specimen in the mechanical database is either directly measured using hot extraction method or indirectly determined based on correlating hydrogen pickup with measured oxide layer thickness.

*Effects of Irradiation and Hydriding*

The CSED model correlates the mechanical state of test specimen at fracture to the hydrogen content, and it is a metric that evaluates the clad ductility. Both irradiation and hydride formation in zirconium alloy can reduce the ductility of cladding tubes. Although irradiation has been considered to be the dominating variable affecting ductility [10], irradiation effects generally saturate at a low fluence level. The selected irradiated fuel cladding has a high fluence level. Therefore, only hydrogen is used as the parameter in the model. Applying the CSED model based on high fluence data would only be conservative for fuels with very low burnup since the irradiation effects on the cladding ductility saturates at a low fluence level.

In the application of the CSED model in Bison modeling, the hydrogen content in the cladding needs to be computed. In the simulated RIA tests, such data are more readily available, and some tests have detailed characterization of the cladding hydrogen content. In Bison modeling, a constant hydrogen pickup ratio is used to convert the oxide layer thickness into the hydrogen content when the hydrogen content cannot be obtained directly from the code.

The hydride distribution could also affect the fracture characteristics; pre-hydrided cladding tube with more hydride concentrated on the outer surface tends to burst at lower pressures as compared to uniformly distributed hydrides in tube burst tests [11]. However, there was not sufficient details to include hydride distribution in the CSED model. Hydride orientation can also affect the cladding ductility. The model developed is for PWR type cladding which are cold-worked stress relieved (CWSR) Zry-4 having the same morphology with predominately circumferentially aligned hydrides. The hydride orientation effect is expected to be similar and is not explicitly modeled. In the case with a Recrystallized annealed material with different hydride orientation, a different model needs to be used.

*Effects of Multi-Axial Loading*

Fan and Koss [12] investigated the fracture of un-irradiated Zry-2 sheet with hydrogen content ranging from 21 to 615 ppm at room temperature under different loading paths: uniaxial, plane strain, and equal-biaxial tension; by converting the fracture strain in rolling and transverse direction into an effective fracture strain, they showed that effective fracture strain under equal-biaxial condition is lower than that obtained under uniaxial tension or plane strain conditions: the higher hydrogen content, the stronger the loading path affects the fracture strain. Based on the work of Fan and Koss, a factor to correct the plane strain condition to equal-biaxial loading path was derived by Leclercq et. al. [13], which is shown as follows:

$$f = 1.03\exp(-0.0006H) \qquad 2)$$

The measured total elongation from mechanical tests (tube burst) was converted to the strain under equal-biaxial tensions using Eq. 2) in the calculation of CSED.

In the Bison RIA modeling, Strain Energy Density (SED) is evaluated at all cladding elements, and the peak values at the cladding outer wall with lower temperature are compared to the CSED which is evaluated based on the cladding corrosion and hydrogen absorption in the cladding tube to determine the failure potential. A comparison to the failure model was reported previously on the simulated RIA tests VA-3, VA-4, and RH-2 [9]. Figure 3 provides an update on the SED/CSED calculations for the CABRI test cases. Maximum SED versus hydrogen content for each test cases from Bison output is plotted in Figure 3 to compare to the CSED model. Two failure cases VA-3 and RepNa-10 are well above the CSED indicating the predicted failure, and most of the non-failure cases are well bounded by the failure curve except for the test case VA-4. Failure predictions are comparable to the Falcon code in Ref. [14].

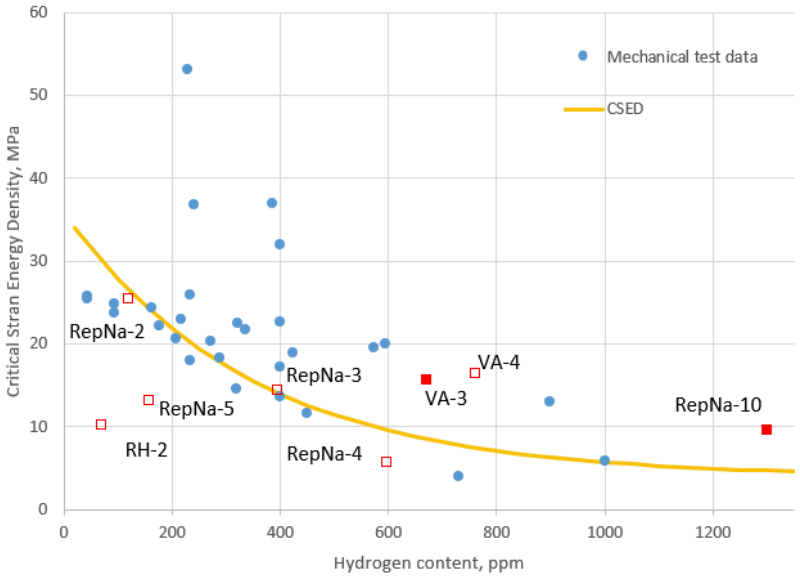


Figure 3: Strain energy density calculated by Bison in comparison to a CSED (as a function of total hydrogen content) failure model; solid symbol represents failure case, and hollow symbol represents non-failure case

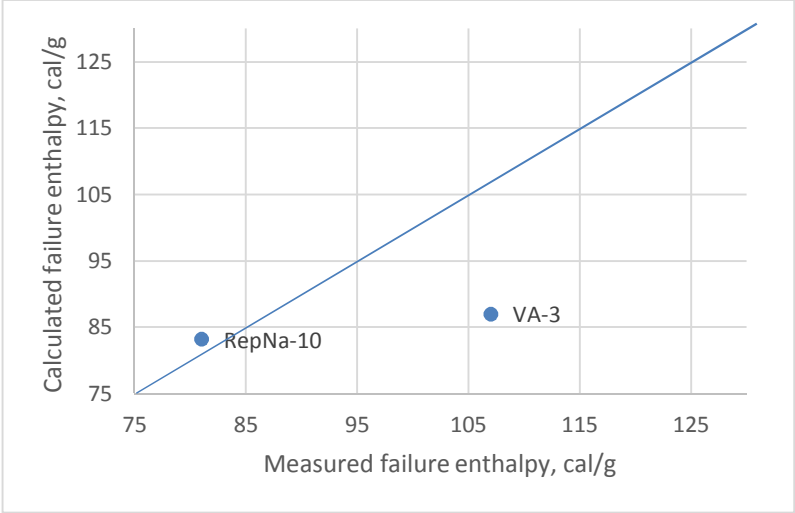


Figure 4: Comparison between Bison calculated failure enthalpy (determined as the enthalpy at predicted CSED) and measurement for the failure cases

The failure enthalpy, determined as the enthalpy at the time that the SED reaches the predicted CSED for the two failure cases, is plotted in Figure 4. Note that the prediction for VA-3, under-estimates the failure enthalpy by ~20 cal/g, while the case RepNa-10, which appears to match closely to the measured failure enthalpy is a case that has spalled oxide and excessive high local hydrogen content. Therefore, the model appears to provide a conservative estimation of PCMI failures in RIAs.

## 2.2 High Temperature Failures

Operation at high cladding temperatures for extended periods of time can lead to cladding failure by several high temperature mechanisms. Concerns for the high temperature failures are the ballooning type of failure due to higher pressure differential across the cladding of high burnup fuel and the high

temperature oxidation and embrittlement of cladding. It is important to accurately predict cladding temperature as both of these failures types correlate strongly with the cladding temperature.

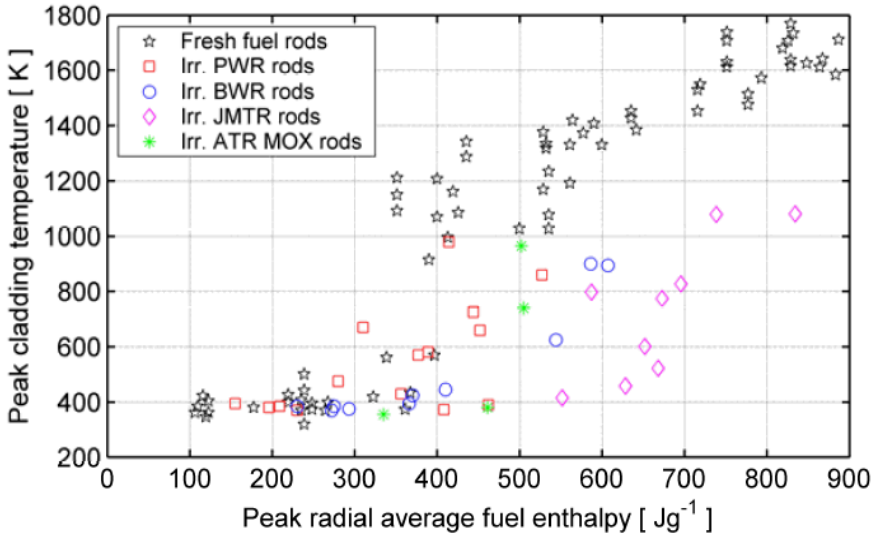


Figure 5: Peak cladding temperature measured in NSRR tests at ambient condition [15]

Figure 5 shows a survey of the peak cladding temperature in NSRR RIA tests [15]. Those results indicate that the threshold to DNB can vary and it appears to range from 70 to 130 cal/g for the refabricated commercial rods (fresh and irradiated) tested in the NSRRs. With the occurrence of DNB, clad could have large deformation at high temperatures driven by the pressure differential across the cladding. Results for low-tin cladding alloy of PWR fuel (irradiated from 38 GWd/tU to 50 GWd/tU) have shown the apparent DNB and large clad ballooning with measured cladding temperature escalation [4].

It should be noted that those tests were primarily conducted at ambient condition with stagnant water. The enthalpies from those results are not directly applicable to PWRs with higher system pressure that could also have higher critical heat flux. RIA tests at IGR and BIGR on VVER fuel show ballooning failure above ~160 cal/g [16, 17], but those tests were also done at ambient condition with stagnant water. RH-2 in NSRR is the only pressurized test at high temperature conditions and it showed DNB with a peak fuel enthalpy of 110 cal/g but no additional information is available to determine a threshold. IRSN tests on clad-coolant heat transfer during fast transients such as RIA indicates that the critical heat flux might be higher [18] compared to slower transients. Also, irradiated fuel with a corrosion layer could also have a higher DNB threshold and better rewetting characteristics [19, 20]. Depending on the duration of the high temperature during film boiling, the fuel rod may remain intact after the rewetting. In fact, many fuel rods reported to go into DNB during the simulated RIA tests in NSRR did not fail. The cladding temperature in the transient would depend on the cladding-coolant heat transfer, clad oxidation, as well as gap conductance, and DNB itself is insufficient to determine the failure. The power pulse from PWR CREAs typical has a broader power shape and tail compared to the power pulse generated for RIA tests, and this may also have implications on DNB and rewetting.

The current work models the RIA using the built-in thermal hydraulics models in Bison code. No attempt is made to re-calibrate the thermal hydraulic models to model the clad rewetting. An accurate modeling of the thermal hydraulics boundary condition is expected to be provided by the VERA COBRA-TF (CTF) for Bison. Also, no specific models were developed for the ballooning type fuel failures at high temperatures in RIAs. The ballooning type of failure is expected to be accounted for in the high temperature visco-plasticity models for the modeling of loss-of-coolant accidents

(LOCAs), and code validations for LOCAs could prove such capability [21]. However, it would still be prudent to model RIA tests with clad ballooning prior to the code application. Note that the impact of the oxide layer on the transient heat transfer is not modeled in current work, but Bison input models could be adapted to add a separate layer of mesh to model the oxidation effect, which could be an area of improvement.

## 3. RIA EXPERIMENTS MODELING

Most of simulated RIA tests (more than a thousand) have been carried out on unirradiated (fresh) fuel, and only about one-tenth of the total tests were done on the irradiated fuels. Several RIA tests that have been performed on rods at high burnups at the CABRI test facility in France and the NSRR test facility in Japan were selected for Bison validation on the RIA modeling.

NSRR is test reactor, in which, a single instrumented fuel rod in a water-filled capsule is placed the core, and is pulse irradiated to simulate the response in a RIA. A large number of experiments on simulated RIA have been performed at the NSRR test facility to evaluate fuel rod behavior and failures at different energy deposition, burnup, fuel design, and coolant condition. Pulse irradiation tests were normally performed in stagnant coolant water at room temperature (~20$^{o}$C) and atmospheric pressure (~0.1 MPa) under a narrow power pulse with FWHM of approximately 5 ms. Recent tests were performed at high coolant temperature (280$^{o}$C) and high pressure (up to 6.4 MPa) to provide measurements on fuel failures at conditions close to temperature at HZP condition. A number of tests on PWR type fuels with high burnups, VA-3, VA-4, and RH-2, were modeled using Bison based on published information from Japan Atomic Energy Agency (JAEA) [9].

The RIA tests conducted at the CABRI test facility have burnups range from 33 to 65 GWd/tU. Twelve test rods (both $UO_2$ and MOX fuel) were performed in the sodium coolant loop. The CABRI test reactor is a pool-type Light Water Reactor (LWR) designed with a central area that can accept the insertion of a test capsule which contains the in-pile instrumentation. The simulated RIA tests for Bison validation include the CABRI REP Na-2, 3, 4, 5, and 10 cases with $UO_2$ fuel. Details of each case, including modeling options and comparisons to experimental data and other code predictions, are summarized in the Bison assessment documents.

Note that all those tests are not representative of the conditions in commercial reactors, as NSRR has a very narrow power pulse (~5 ms) and stagnant coolant water, and CABRI sodium coolant test loop cannot simulate DNB and the high temperature failures.

Previous Bison RIA modeling has shown good agreement between the Falcon code and Bison code results on the fuel temperatures [22]. However, since those validations were performed using a frictionless contact model due to the numerical issues with the frictional contact algorithm in Bison, the mechanical deformations calculated by Bison are less satisfactory. Recent updates have been performed on all the tests using the frictional contact method. Bison calculated characteristics on the NSRR high temperature cases and CABRI sodium test loop cases are summarized in the Table **1** and Table **2** respectively.

Table 1: Summary of the Bison calculated characteristics for the NSRR cases in comparison with measurements and Falcon calculations [9]

| **Test case** | **VA-3** | **VA-4** | **RH-2** |
|---|---|---|---|
| Permanent Hoop Strain (%) | 1.06 | 1.05 | 0.80 |
| Peak Hoop Strain (%) | 1.65 | 1.65 | 1.41 |
| Plastic Axial Strain (%) | 1.4 | 1.32 | 0.76 |
| Initial Fuel Enthalpy (cal/g) | 24.49 | 22.048 | 22.516 |
| Peak Fuel Enthalpy (cal/g) | 131.59 | 131.09 | 110.97 |

| | | | |
|---|---|---|---|
| Enthalpy rise (cal/g) | 107.1 | 109.04 | 88.45 |
| Measured Max. Cladding Permanent Hoop Strain (%) | NM | 2.2 | 1.06 |
| Falcon Calc. SED (MPa) | 16.1 | 16.5 | 10 |

Table 2: Summary of the Bison calculated characteristics for the CABRI cases in comparison with measurements and Falcon calculations [8]

| **Test case** | **RepNa-2** | **RepNa-3** | **RepNa-4** | **RepNa-5** | **RepNa-10** |
|---|---|---|---|---|---|
| Permanent Hoop Strain (%) | 1.28 | 0.62 | 0.06 | 0.57 | 0.52 |
| Peak Hoop Strain (%) | 1.75 | 0.97 | 0.82 | 1.18 | 1.12 |
| Peak Clad Elongation (mm) | 13.83 | 5.88 | 3.37 | 6.22 | 5.95 |
| Peak Fuel Enthalpy (cal/g) | 208.46 | 136.72 | 87.77 | 117.60 | 118.73 |
| Max. SED (MJ/m3) | 25.58 | 14.42 | 5.83 | 13.07 | 9.57 |
| Measured Peak Cladding Permanent Hoop Strain (%) | 3.5 | 2.2 | 0.4 | 1.1 | NM |
| Falcon Calc. Perm Hoop Strain (%) | 2.13 | 0.995 | 0.233 | 0.718 | 0.637 |
| Falcon Calc. SED (MPa) | 28.2 | 16.6 | 5.2 | 12.5 | 10.9 |

The calculated permanent hoop strains are still lower than measurements in general for both NSRR and CABRI cases, but comparable to Falcon results. The clad elongation prediction is much improved. Figure 6 shows the calculated clad elongation for both Bison and Falcon for CABRI cases in comparison to the measurement. The Bison calculations appear to be in good agreement with measurement, which also shows the successful modeling of the frictional contact between pellet and cladding for RIA. While the measured clad elongations are not available from the NSRR experimental results, the calculated plastic axial strains are close to the plastic hoop strains, which also indicates that the strong PCMI was modeled as a result of the friction between pellet and cladding in the simulated RIA.

Figure 7 shows that the max SEDs computed by Bison and Falcon are very close for all the NSRR and CABRI cases, and that the trend lines show a small variation (< ~2MPa). Note that some differences could be attributed to the relatively larger pellet-clad gap prior to the RIA calculated in the Bison models compared to the smaller gap size assumed for Falcon RIA modeling results.

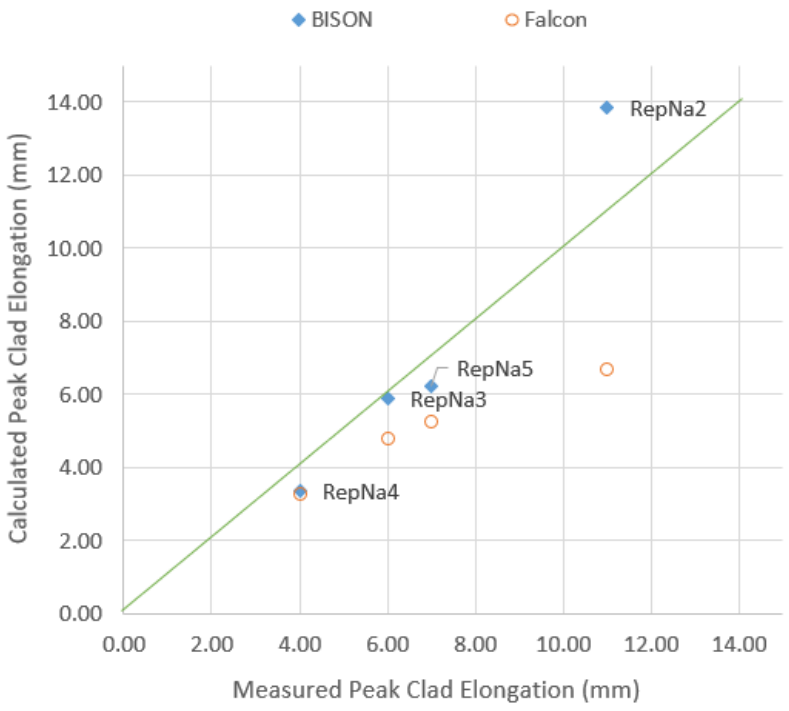


Figure 6: Comparison between calculated and measured peak clad elongation for Bison and Falcon

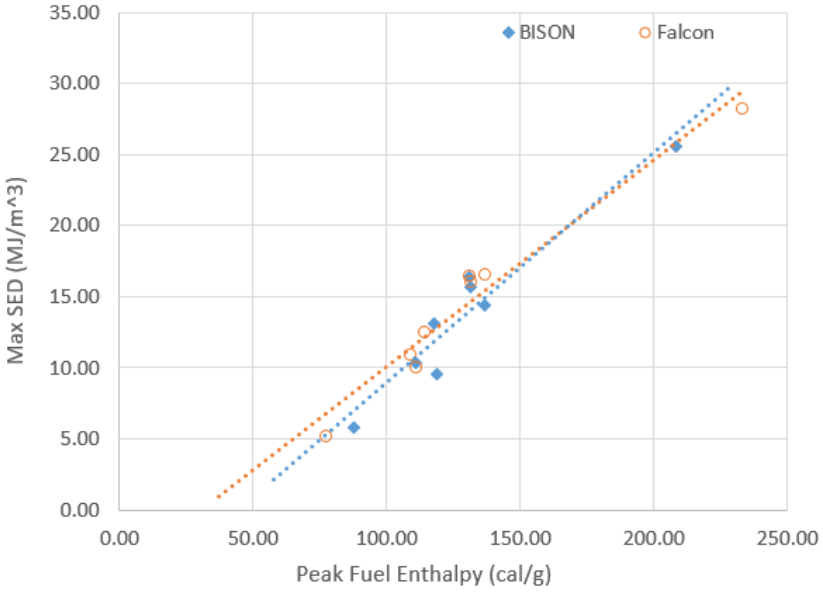


Figure 7: Comparison between Bison and Falcon calculations of strain energy density for CABRI and NSRR cases

Current results from Bison code have shown good agreement in benchmarking against Falcon code, while underestimation of some mechanical response, similar to Falcon prediction, such as the cladding permanent hoop strains in the measurement indicates that there is still a gap between the calculation and measurement. The Bison code overall has shown a good capability in the modeling of the RIA tests with peak fuel enthalpies ranging from ~90 cal/g to ~210 cal/g for high burnup fuels.

# 4. MODELING PWR REA

## 4.1 NEA benchmark case description

The transient power history and axial power profile used for the analysis are generated from neutronic code, PARCS, output for benchmark cases developed for simulating the rapid ejections of a control assembly (CA) at HZP condition [6,7]. This provides a more realistic simulation of power pulse for the analysis of fuel thermal-mechanical responses in REA condition.

Ongoing CASL activities on VERA whole core simulation could provide the fuel rod powers with various reactivity insertion at different burnup levels, but the current investigation is focused on the fuel performance modeling using Bison. Two benchmark cases were selected: a) case A1 represents a case with central control rod ejection, which has inserted reactivity of $1.08 and features a relatively lower level of power and wider power pulse (160 ms), and b) case C1 represents a case with peripheral rod ejection, which has inserted reactivity of $1.24. The neutronic characteristics for the REA cases are shown in Table 3. Figure 8 shows the core map and the locations of ejected control assemblies. Those cases (A1 and C1) did not model the reactor trip; the power is reduced to zero after 5 sec in the Bison input. According to [23], the resulting change in maximum fuel enthalpy (defined for a no-trip case at 3 s) is only ~2 cal/g for a case with inserted reactivity of $1.2. Therefore, the peak fuel enthalpy computed is expected to be slightly higher than a case with a reactor trip. The fuel enthalpy right after the prompt energy deposition is closer to the peak fuel enthalpy of a RIA case with a reactor trip, and all the thermal and mechanical responses up to the time of prompt energy depositions are still valid for examining the fuel responses with a reactor trip. The core relative power for cases A1 and C1 is shown in Figure 9.

Table 3: Neutronic characteristics of REA cases

| Case | Pulse width (ms) | Peaking Factor | Reactivity ($) |
|---|---|---|---|
| A1 | 160 | 1.26 | 1.08 |
| C1 | 50 | 4.82 | 1.24 |

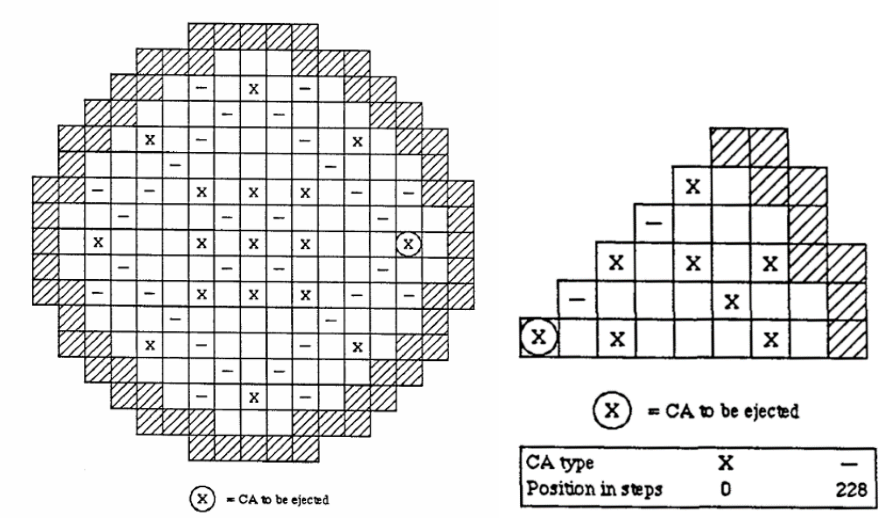


(a) Case C1 (b) Case A1

Figure 8: Core map for the simulated control rod ejection accidents at hot zero power condition: a) Case A1, peripheral control assembly is ejected, and b) Case C1, central control assembly is ejected [6]

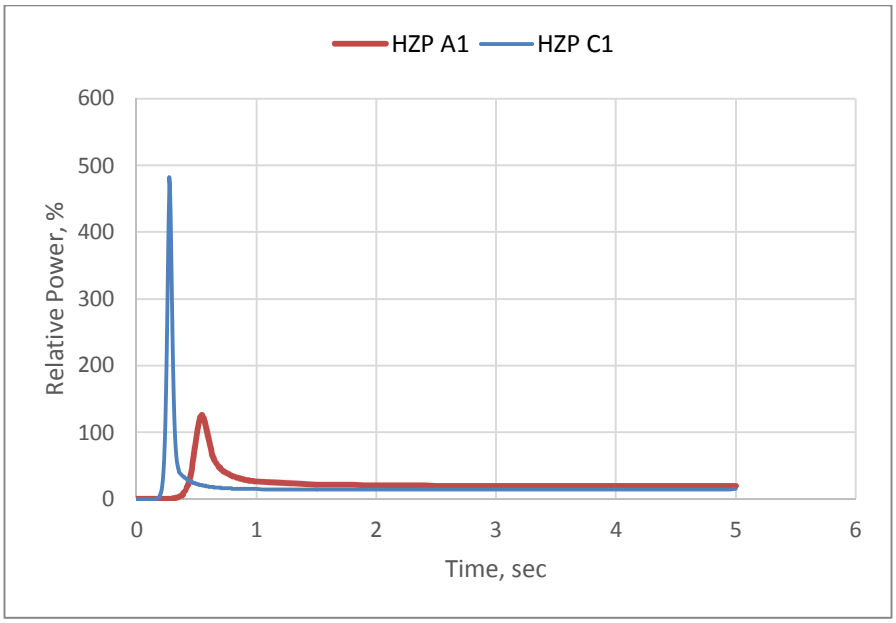

Figure 9: Core relative power for case A1 and case C1

The fuel design and operation parameters at HZP condition are listed in Table **4**.

Table 4: Design and operation parameters

| **Parameter** | **Value** | **Unit** |
|---|---|---|
| Clad thickness | 0.571 | mm |
| Fuel stack length | 3.66 | m |
| Rod pitch | 12.66 | mm |
| Enrichment | 4.5 | % |
| Fuel material | $UO_2$ | - |
| Clad material | SRA Zr-4 | - |
| Coolant inlet temperature | 286 | $^oC$ |
| Coolant pressure | 15.5 | MPa |
| Coolant mass flux | 3143 | $kg/m^2$-sec |
| Fuel surface roughness | 1.0 | micron |
| Clad surface roughness | 1.0 | micron |

## 4.2 Bison Input Models

A 2-D radial axisymmetric geometry with eight-node quadratic element is used to model the RIA test case. Biased meshing is used to model the fuel column with a finer mesh at the pellet rim and a coarser mesh at the central region to capture the edge-peaked radial power/burnup profiles of high burnup fuels. In the radial direction, four columns of elements are used for meshing the cladding to capture the steep temperature gradient in the fast transient. A schematic of the mesh used for the RIA test case is shown in Figure 10 below. A uniform axial burnup profile is assumed for this case.

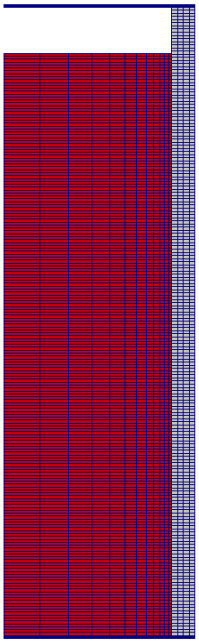

Figure 10: Finite element mesh used for the PWR REA case

Figure 11 shows the rod average linear heat rate during the RIA. Figure 12 shows the axial power profile at a few selected time steps during the simulate accident.

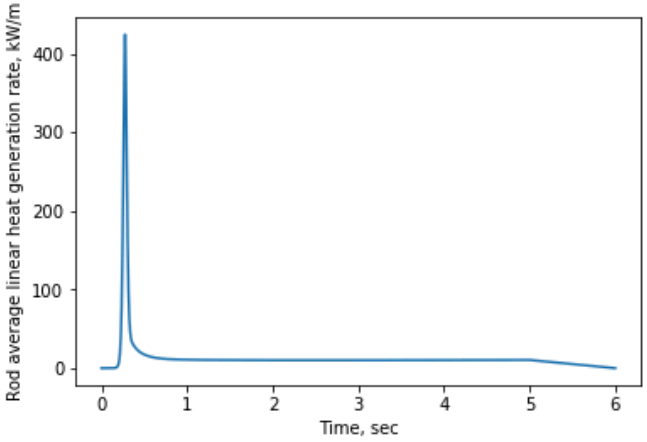


Figure 11: Power pulse history of case C1 during the RIA (Peak LHGR = 424.35 kW/m)

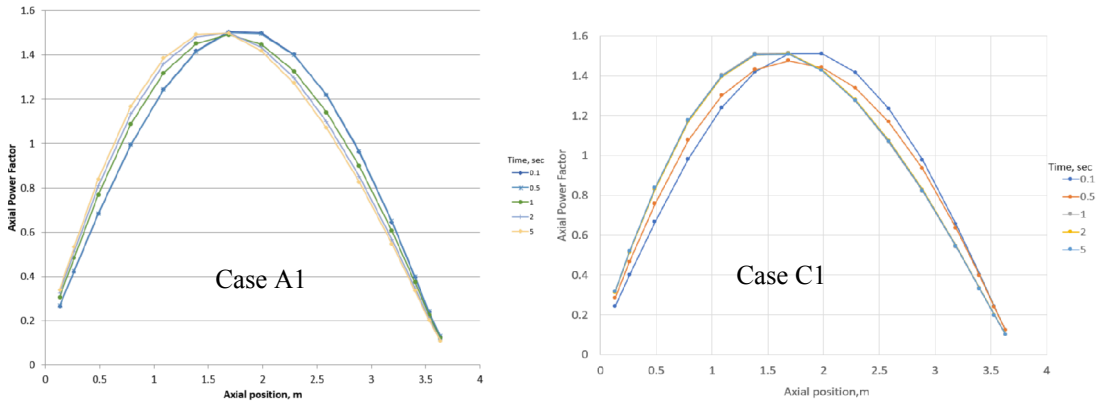


Figure 12: Axial power profiles for the test cases A1 and C1

Key input parameters and assumptions for Bison input models are summarized in Table 5.

Table 5: Bison input models

| **Model** | **Parameters** |
|---|---|
| Fuel thermal conductivity | NFIR |
| Fuel mechanical model | Elastic model |
| Clad mechanical model | Instantaneous plasticity model |
| Frictional coefficient | 0.4 |
| Fission gas release and swelling | Not modeled |
| Heat transfer correlations:<br>Liquid convection<br>Nucleate boiling<br>Film boiling<br>Critical heat flux | <br>Dittus-Boelter correlation<br>Thom correlation<br>Bishop-Sandberg-Tong correlation<br>BIASI correlation |
| Geometry | 2-D radial axisymmetric |
| Fuel mesh<br>Clad mesh | 12 (radial) x 200 (axial)<br>4 (radial) x 200 (axial) |
| Element type | Quad-8 |

*Clad yield stress model*

EPRI clad yield stress model for SRA Zr-4 was used in the modeling of the instantaneous plastic deformation of Zircaloy cladding. The model was developed for high burnup fuel which has an applicable range up to ~$10^{26}$ n/$m^2$. It is the same model used in Falcon fuel performance code.

*Gap conductance model*

The gap conductance consists of the gas conduction, solid-solid contact, and radiation conductance. Details on the model are described in Bison theory manual [24].

*Radial power/burnup profile model*

The model to compute radial power and burnup distribution in fuel pellets in Bison are based on several subroutines to solve fission isotope generations using an effective one group cross sections. The model was developed for the DIONISION code and was described in Ref. [24, 25]. This model was validated against high burnup data with an applicable average burnup for LWR $UO_2$ fuel up to 150 GWd/tU [25].

*Cladding corrosion model*

Bison code has implemented EPRI KWU/CE model for the modeling of cladding corrosion in the base irradiation condition, described in [24]. For the SRA Zr-4 type of cladding, the corrosion rate calculated had been assessed for a number of commercial PWR fuels, and reasonable agreement was achieved as shown in Bison assessment documents. In the validation of base irradiation of CABRI test cases, the cladding corrosion can be reasonably predicted by the corrosion model, as shown in Figure 13.

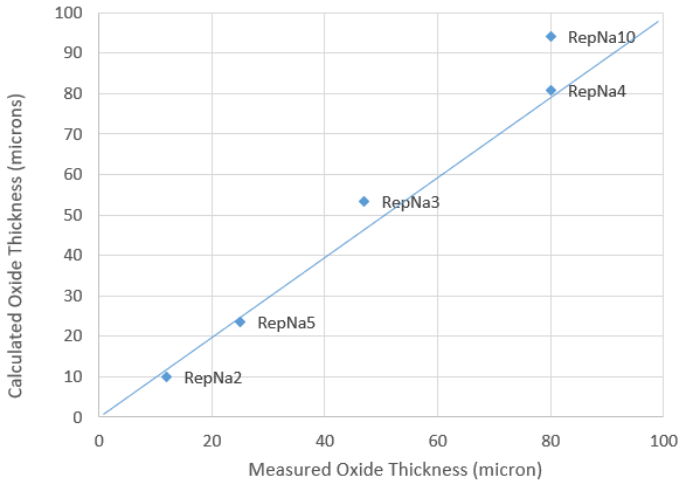


Figure 13: Bison calculated maximum oxide thickness in comparison to measurement

## 4.3 Initial Burnup Condition

The conditions prior to the simulated RIA are modeled using typical PWR fuel end of cycle conditions at different burnup levels shown in Table 6. Note that the variations of those parameters exist at same burnup level, and the current investigation is only limited to one set of parameters for a PWR fuel showing a general dependency on burnups. As will be seen, that some parameters, e.g. gap size, which could vary substantially, would be important in determining the response in the RIAs. Figure 14 shows the gap size versus burnup from both measurements and code calculations, which shows the large scattering, but generally reduces to zero at high burnup.

Table 6: Fuel characteristics at different burnup levels

| **Rod Average Burnup, GWd/tU** | **0** | **20** | **40** | **60** |
|---|---|---|---|---|
| Density, kg/m$^3$ | 10521.6 | 10431.06 | 10304.38 | 10180.75 |
| Fractional density, %TD | 0.96 | 0.9517 | 0.9402 | 0.9289 |
| Pellet outer diameter, mm | 8.239 | 8.263 | 8.297 | 8.331 |
| Gap size, micron | 80 | 16 | 8 | 0 |
| Fluence, $10^{22}$n/cm$^2$ | 0 | 0.339 | 0.678 | 1.00 |
| Gap gas: He, % | 100 | 99.86 | 99.68 | 96.43 |
| Xe, % | 0 | 0.14 | 0.32 | 3.0 |
| Kr, % | 0 | 0 | 0 | 0.57 |
| Rod internal pressure, MPa | 2 | 2.5 | 3 | 4 |

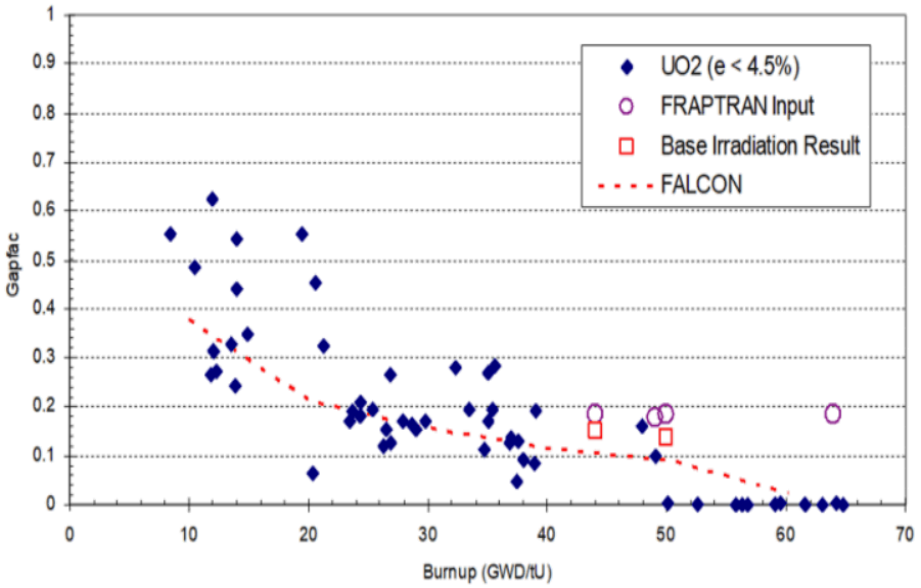


Figure 14: The gap factor (ratio of cold gap size to as-fabricated gap size) for irradiated fuel, determined from code calculation and measurement data [26]

The radial burnup profile and radial power profile were calculated using Bison model, and those profiles were scaled to the geometry of the irradiated fuel for the RIA simulation. The radial burnup profile and radial power profile at different burnups are shown in Figure 15 and Figure 16, respectively.

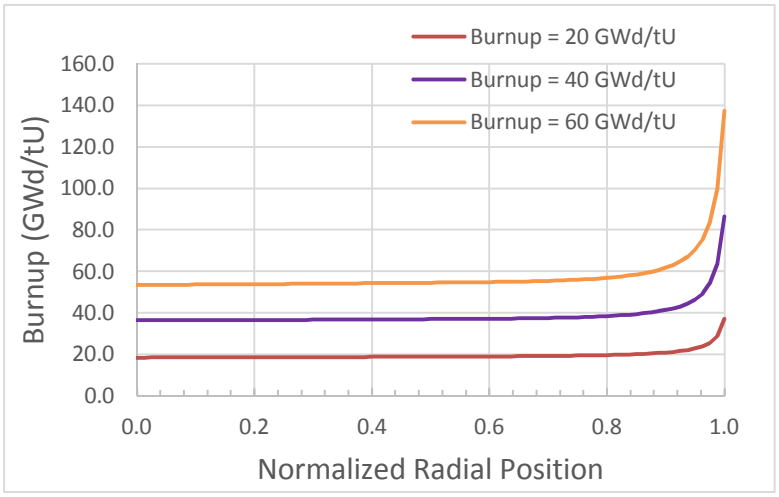


Figure 15: Radial burnup profile at different burnups of 20, 40, and 60 GWD/tU

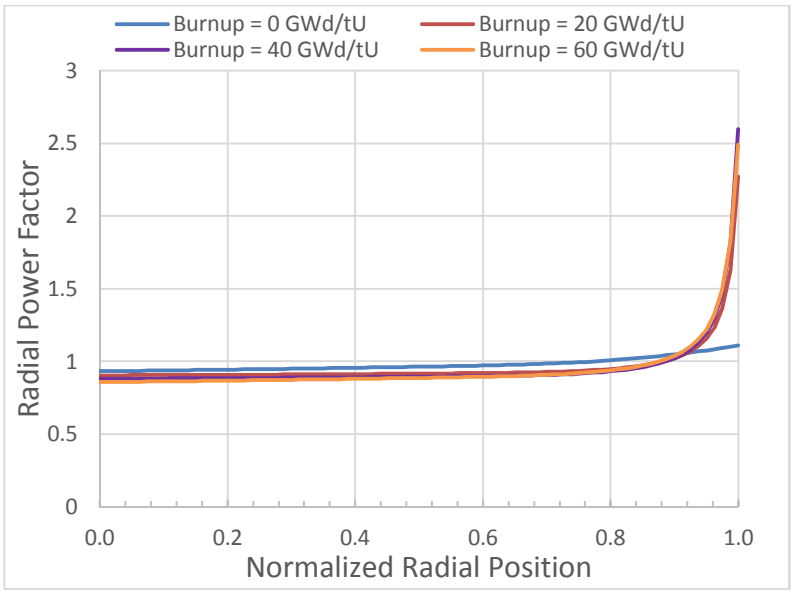


Figure 16: Radial power profile at different burnups of 0, 20, 40, and 60 GWD/tU

The failure model was correlated to the hydrogen absorbed in the cladding from the base irradiation, A constant hydrogen pickup ratio of 0.15 is used to convert the oxide layer thickness calculated by Bison into the hydrogen content in the cladding. An equation, from the calculation of the hydrogen pickup of the cladding tube with a thickness of 0.57 mm, is derived, and simplified in a polynomial form to convert the oxide thickness, $t_{ox}$(micron), into the hydrogen content, $H_{0.15}$(ppm), shown as follows:

$$H_{0.15} = 0.0097t_{ox}^2 + 7.2859t_{ox} + 15.817 \quad 3)$$

The oxide thickness calculated using Bison and converted to hydrogen content for a PWR fuel irradiated up to 60 GWd/tU is shown Figure 17. The peak values for the calculated hydrogen content are used to determine the CSED for the comparison to the Bison RIA modeling.

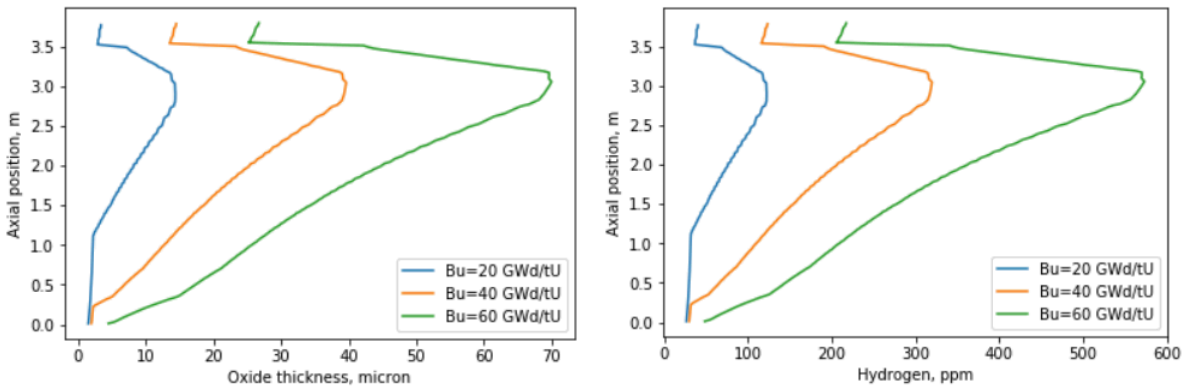


(a) Oxide thickness (b) Hydrogen content

Figure 17: Calculated oxide thickness and hydrogen content in a PWR fuel at different burnup

The calculated hydrogen content (maximum and average) and CSED at different burnup levels are also shown in Table 7 below. The most limiting cases of CSED are at high burnup: 10 MPa with 15% hydrogen pickup (573 ppm hydrogen) and 5.1 MPa with 30% hydrogen pickup (1156 ppm hydrogen) at the rod average burnup of 60 GWd/tU.

Table 7: Calculated CSED and hydrogen content at different burnup levels: 20, 40, and 60 GWd/tU

| **Rod Avg. Burnup, GWd/tU** | **20** | **40** | **60** |
|---|---|---|---|
| Rod average hydrogen content, ppm | 65.1 | 175.0 | 317.0 |
| Maximum hydrogen content, ppm | 122 | 320 | 573 |
| *CSED with 15% hydrogen pickup, MPa | 26.3 | 16.7 | 10.0 |
| *CSED with 30% hydrogen pickup, MPa | 19.7 | 9.0 | 5.2 |

**CSED is calculated using maximum hydrogen content*

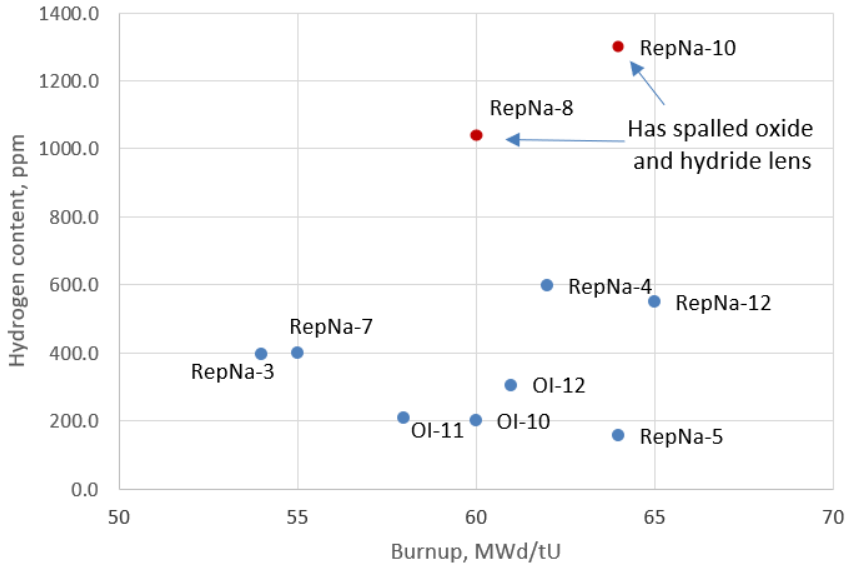


Figure 18: Hydrogen content in test rods in CABRI and NSRR tests at high burnup

Figure 18 shows measured hydrogen content from simulated RIA tests, reported in [14]. CABRI RepNa-8 and RepNa-10, which had areas of spallation allowing for the formation of a hydride lens, are the exceptions to the other data, and are not considered typical due to the hydride lens. The hydride lens occurs after the spalling of the oxide, which results in better heat transfer at the cladding surface creating a cold spot allowing more hydrogen to diffuse to that area and precipitate locally. The maximum hydrogen content of all other cases, at high burnup 60–65 GWd/tU, is ~600 ppm comparable to the calculated values in Table 7.

# 5. PWR REA RESULTS

## 5.1 Results for the base case

Figure 19 plots the comparison of the peak fuel radial average enthalpy between case A1 and C1, a) plots the response up to 20 sec, and b) is a zoom-in of the plot of enthalpy between 0 and 5 sec. Case C1 has a narrower pulse width than case A1, resulting in a faster enthalpy increase in the fuel as compared to the case A1. However, the peak fuel enthalpy and cladding hoop stress appears to be similar. This could be attributed to the energy deposition in the power pulse tail, which is constant, and is higher in A1 than C1, due primarily to the lack of reactor trip in the power pulse. The case C1 will be evaluated in detail in the subsequent sections. The enthalpy at approximately 0.5 sec is

estimated to be the enthalpy with a prompt energy deposition in the case C1. The fuel and cladding temperatures are shown in Figure 20.

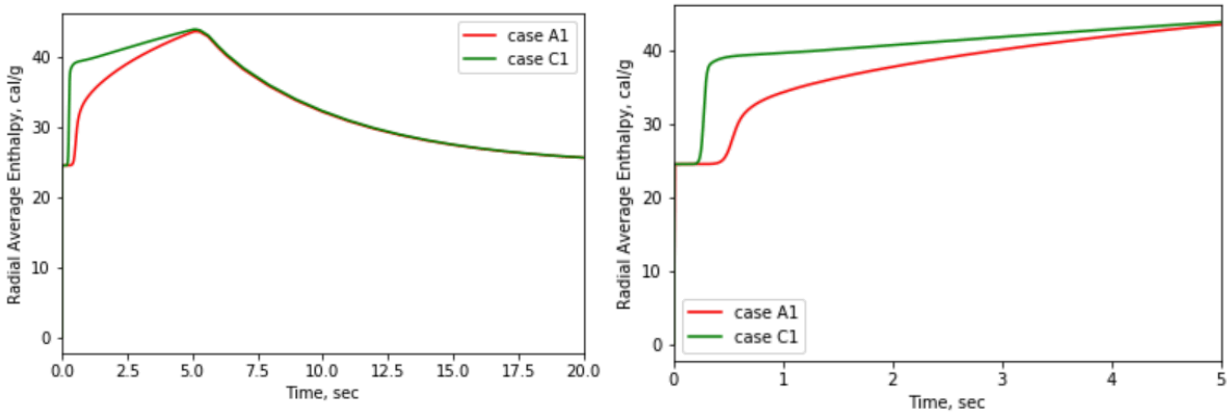


(a) response up to 20 sec b) zoom-in

Figure 19: Comparison between case C1 and A1 on peak fuel radial average enthalpy

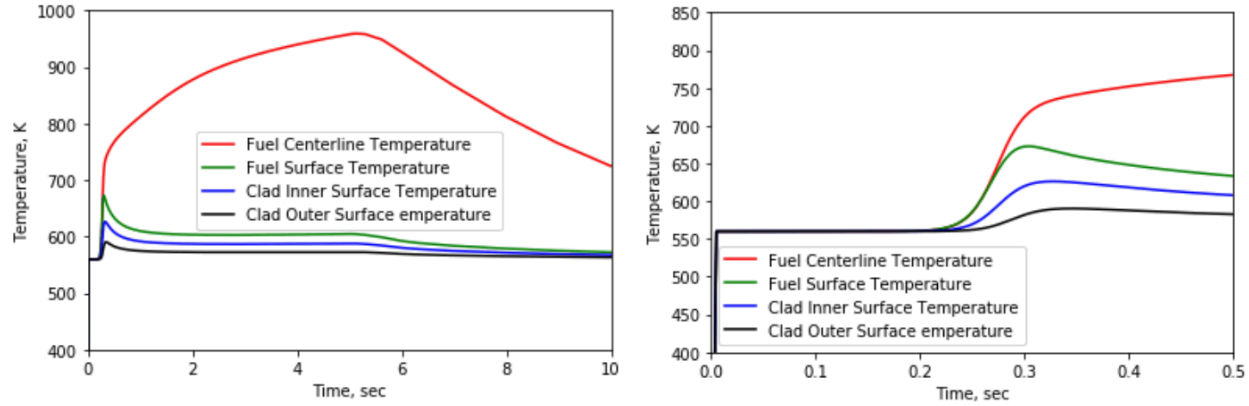


(a) response up to 10 sec b) zoom-in

Figure 20: Fuel centerline, fuel outer surface, clad inner and outer surface temperatures

## 5.2 Fuel thermal and mechanical responses at different burnups

Figure 21 - Figure 25 below shows a comparison of fuel thermal and mechanical responses at different burnups during RIA for test case with inserted reactivity of $1.24 with the same power history in the transient.

The rapid power increase causes a prompt fuel enthalpy increase in ~100 ms, and then a gradual increase until 5 seconds due to the shape of the power pulse tail as shown in Figure 21. For irradiated fuel, it appears that the peak fuel enthalpy increases with burnup indicating the effect of fuel thermal properties; higher burnup has lower thermal conductivity and diffusivity, however the difference is small in the stage with prompt enthalpy increase. The case with zero burnup gives the highest enthalpy. An examination of the fuel-clad gap conductance in Figure 22 shows that the case with zero burnup has low gap conductance with a large open gap; the heat transfer from fuel to clad is less than the other cases, and consequently this case has higher fuel temperature and enthalpy.

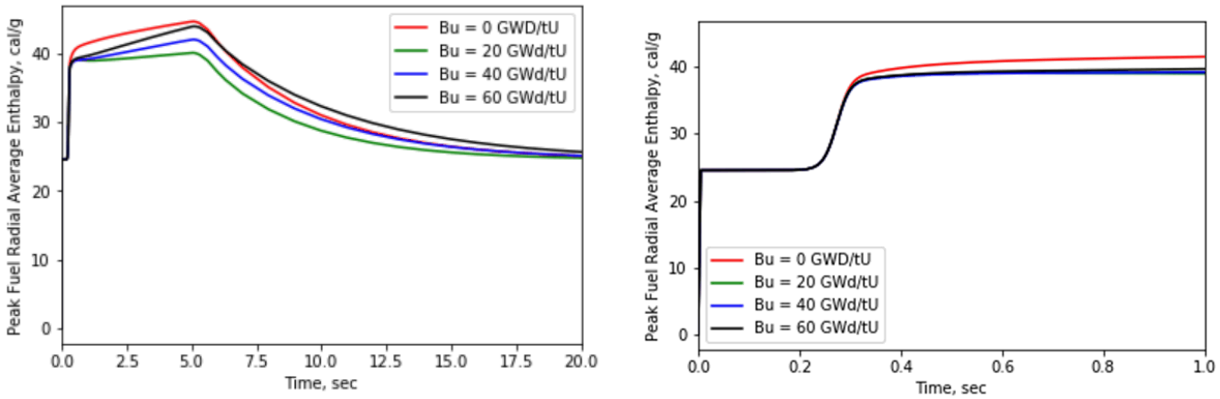


(a) 0-20 sec (b) 0-1 sec

Figure 21: Peak radially averaged fuel enthalpy at different burnups

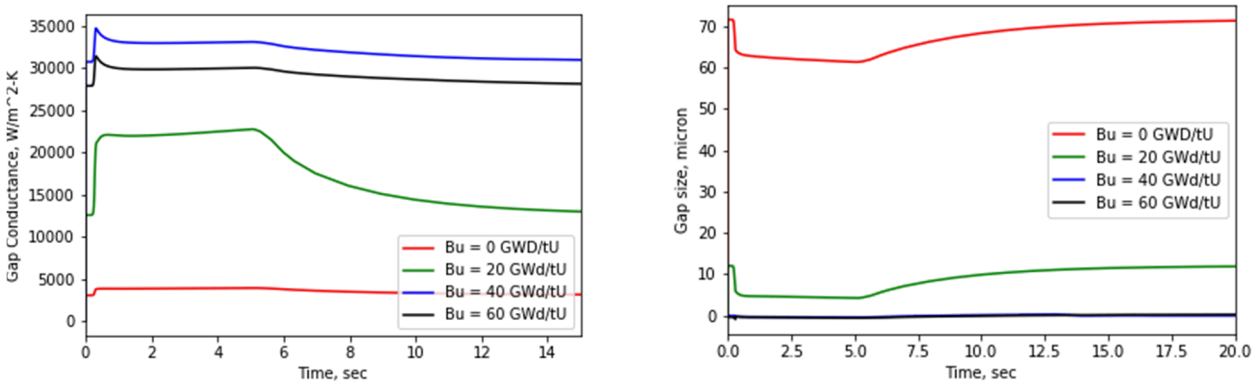


(a) Gap conductance (b) Gap size

Figure 22: Gap conductance and gap size in simulated RIA at different burnups

Figure 23 shows the fuel centerline and outer surface temperature respectively. The fuel centerline temperature also shows the same trend with the increase of burnup at the burnup level of 20, 40, and 60 GWd/tU, but the fresh fuel case appears different, due to the low gap conductance and flat radial power profile in the pellet. Though the edge-peaked radial power profile of irradiated fuel may result in higher fuel outer surface temperature, the fuel clad gap conductance affects the fuel pellet surface heat transfer to the cladding, and the highest fuel outer surface temperature is seen in the fresh fuel case with low gap conductance.

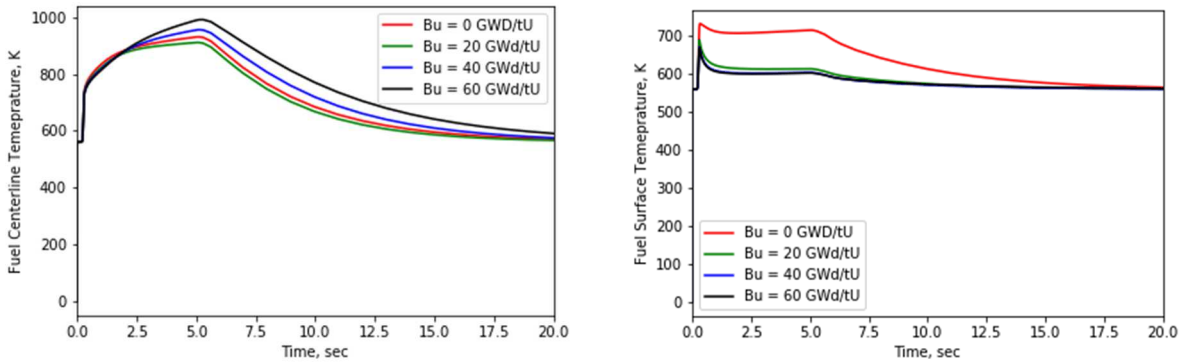


(a) Centerline (b) Fuel Outer Surface

Figure 23: Fuel centerline and outer surface temperature at different initial burnup during RIA

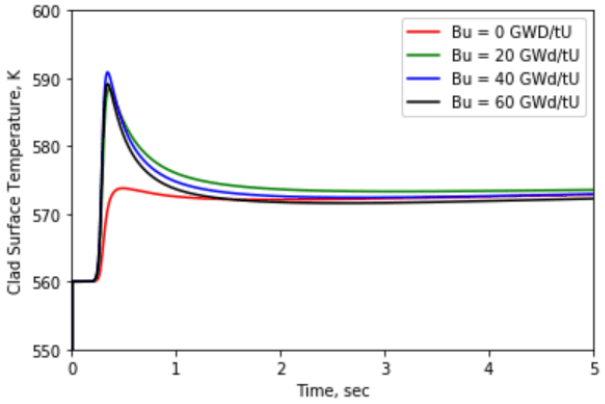


Figure 24: Clad surface temperature at different burnups

Clad surface temperatures at different burnups are shown in Figure 24. The surface temperature increase is consistent with other fuel thermal responses; the fresh fuel case shows lower temperature increase than the other cases.

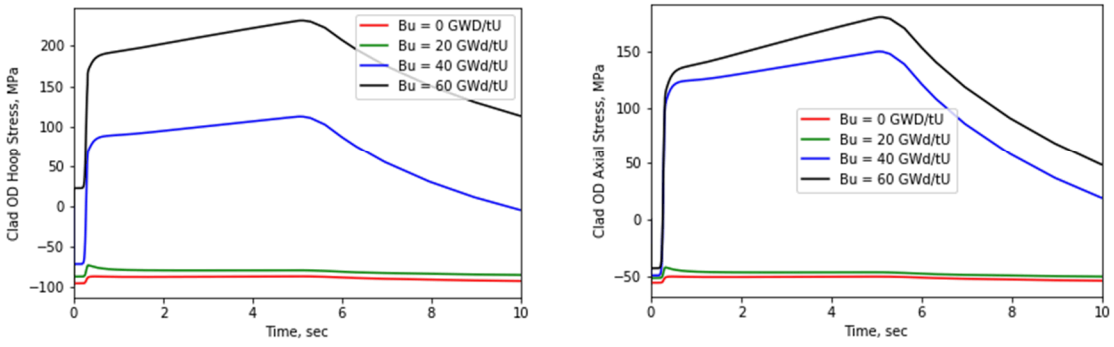


**(a) Hoop Stress** **(b) Axial Stress**

Figure 25: Clad outer surface hoop and axial stress at different burnups

The mechanical responses of the clad outer surface hoop and axial stresses are shown in Figure 25. The cases with 40 and 60 GWd/tU has PCMI due to the gap closure, but stresses are below the clad yield stress, and there is no plastic deformation. Figure 26 shows the strain energy density calculated

for the different cases. The maximum SEDs for burnup at 40 and 60 GWd/tU are well below the CSED for the high burnup fuels.

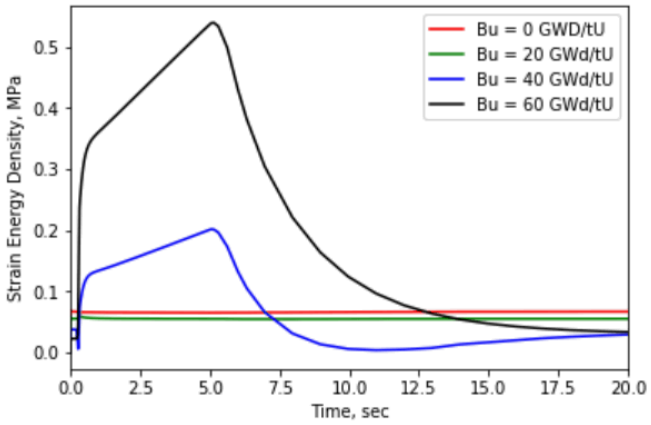


Figure 26: Clad outer surface strain energy density at different burnups

## 5.3 Scaling to high powers

The base case C1 used in the current study has a maximum reactivity insertion of $1.24, which has limited the energy deposition into the fuel. To get the responses of interest to fuel failures, a simple scaling of the magnitude of the power is used to generate higher energy depositions in the fuel. The scaling does not account for the change in the power pulse width, for which a neutronic code output would be needed to provide more realistic power histories in the RIAs, and those inputs can be computed by VERA.

Table 8 provides results of clad mechanical and thermal responses at different scaled powers at the burnup of 60 GWd/tU. It is observed that at high powers, the peak cladding temperature can escalate due to the film boiling. At such condition, the SED computed is no longer a valid metric for PCMI failure. In the film boiling regime, the heat transfer deteriorates, and fuel enthalpy may increase significantly.

Table 8: Results of clad mechanical and thermal responses at different peak powers at the burnup of 60 GWd/tU

| Peak power, kW/m | Peak Fuel Enthalpy, cal/g | Max Clad OD SED, MPa | Max Fuel Radial Displacement, micron | Peak Clad Temperature, K | Peak Fuel Centerline Temperature, K |
|---|---|---|---|---|---|
| 424.4 | 43.9 | 0.4 | 21.0 | 589.2 | 990.9 |
| 636.5 | 53.9 | 1.0 | 26.4 | 604.0 | 1204.7 |
| 848.7 | 64.0 | 1.9 | 32.2 | 619.0 | 1415.2 |
| 1060.9 | 74.1 | 3.1 | 38.0 | 624.1 | 1627.6 |
| 1273.1 | 84.3 | 4.6 | 44.2 | 624.9 | 1838.5 |
| 1485.2 | 94.4 | 6.3 | 50.6 | 625.7 | 2041.5 |
| 1527.7 | 96.5 | 6.6 | 51.9 | 625.8 | 2080.7 |
| 1570.1 | 98.5 | 7.0 | 53.2 | 625.9 | 2119.3 |
| 1612.5 | 100.6 | 7.3 | 54.4 | 626.1 | 2157.3 |
| 1655.0 | 150.3 | 6.0 | 84.2 | 1449.7* | 2334.6 |

* *Case with DNB*

Table 9: Results of fuel enthalpy, clad outer surface SED and temperature at 0.5 sec for the case with 60 GWd/tU

| Peak power, kW/m | Fuel Enthalpy, cal/g | Clad OD SED, MPa | Clad OD Temperature , K |
|---|---|---|---|
| 424.4 | 39.1 | 0.3 | 581.4 |
| 636.5 | 46.4 | 0.6 | 592.1 |
| 848.7 | 53.7 | 1.0 | 602.7 |
| 1060.9 | 61.0 | 1.7 | 612.8 |
| 1273.1 | 68.3 | 2.4 | 621.2 |
| 1485.2 | 75.6 | 3.5 | 623.6 |
| 1527.7 | 77.1 | 3.7 | 623.6 |
| 1570.1 | 78.5 | 3.9 | 623.7 |
| 1612.5 | 80.0 | 4.2 | 623.8 |
| 1655.0 | 83.8 | 3.2 | 928.6* |
| 1697.4 | 85.5 | 3.3 | 960.1* |

* *Case with DNB*

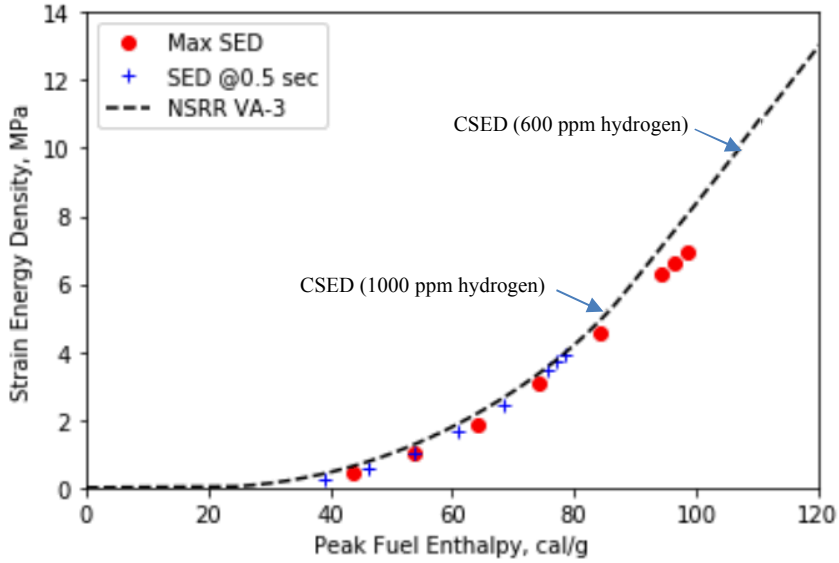


Figure 27: Maximum strain energy density at different fuel enthalpies

To examine whether this is caused by the power pulse tail, the results of SED and clad surface temperature at 0.5 sec, which is considered as the time that is right after prompt energy deposition, are provided in Table 9. It shows that the DNB occurs in the prompt energy deposition stage, and additional energy deposition in the power pulse tail without trip would sustain the cladding temperature increase. One of the case (x4 power) fails to converge due to excessive high temperature, and the results are only shown for the prompt energy deposition in Table 9. However, for RIA with a reactor trip, the response after the prompt energy deposition would differ, and the cladding temperature may reduce as less energy is generated from the fuel to heat up the cladding.

The maximum SED versus peak fuel enthalpy for the case without DNB is plotted in Figure 27. In comparison, the SED @ 0.5 sec, which is considered as the SED with prompt energy deposition, and the SED versus enthalpy from the simulated RIA case NSRR VA-3 (with a burnup of 70 GWd/tU), is also plotted. Though the scaling without adjustment of the power pulse width and the power pulse tail may cause higher fuel enthalpy for the same mechanical deformation, the deviation from the results of an almost adiabatic power pulse (~5 ms) is small. Figure 27 shows that with a very conservative estimate, the PCMI failure enthalpy would be in the range of ~90–110 cal/g. Figure 28 plots the peak fuel enthalpy rise (for an end of cycle case) versus inserted reactivity from Diamond's study [23]. At the inserted reactivity of $2.0, the enthalpy rise is ~55 cal/g, and the peak fuel enthalpy would be ~80 cal/g, still lower than the failure enthalpy.

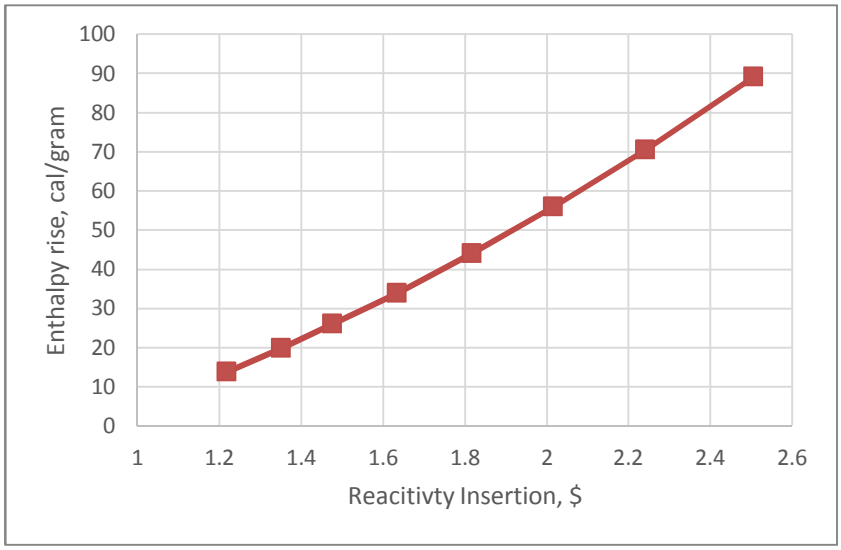


Figure 28: Maximum fuel enthalpy rise for REA at HZP [23]

At a scaled power (x3.5), with a peak power of 1485.2 kW/m, the comparison is made between the 40 GWd/tU case and 60 GWd/tU case, and results are shown in Figure 29. The high burnup (60 GWd/tU) case shows higher SED and higher fuel enthalpy than the 40 GWd/tU case, which is consistent with results at lower powers. Figure 29 (c) and (d) show that the high burnup case has lower gap conductance despite the higher contact pressure. This could be caused by the fission gas xenon modeled in the fill gas to simulate the end of life gas composition. Note that no transient fission gas release is modeled. Fission gas release, if any in the RIA, could change the gap conductance as well.

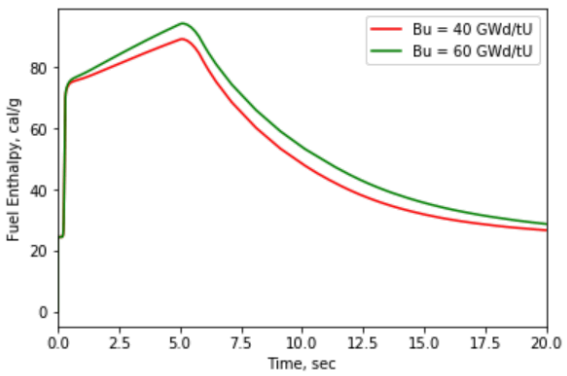


(a) Fuel Enthalpy

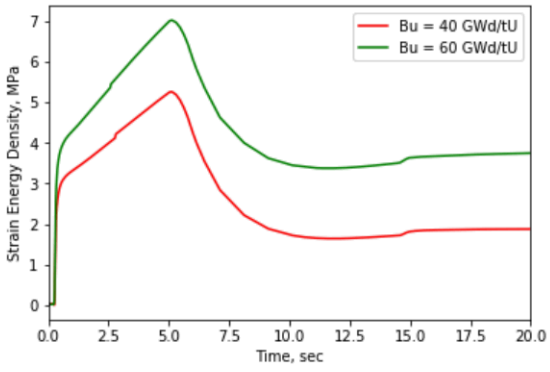


(b) SED

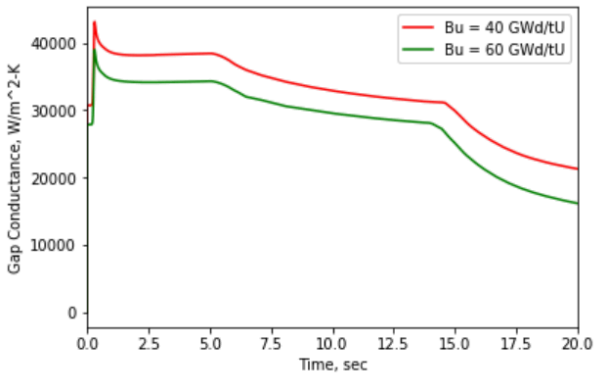


(c) Gap conductance

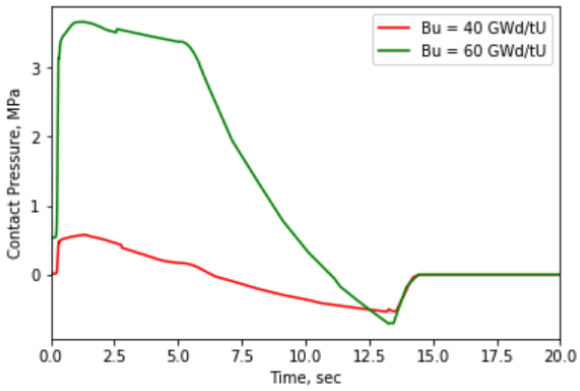


(d) Contact Pressure

Figure 29: Comparison on the thermal and mechanical responses between 40 GWd/tU and 60 GWd/tU at scaled high power

## 5.4 Modeling high temperature failures

Concerns for the high temperature failures are a) the ballooning type of failure due to higher pressure differential across the cladding of high burnup fuel, and b) the high temperature oxidation and embrittlement of cladding. No fission gas release is modeled in current study, only cladding temperature escalation is modeled using boundary conditions in Bison coolant channel model. The coolant enthalpy calculation is turned off. Therefore, it expected that the calculated Critical Heat Flux (CHF) could be higher due to a relatively lower coolant temperature. Also due to the limited power and enthalpy in the reference case, the DNB can only be simulated by scaling the powers to increase the fuel energy deposition.

Figure 30 shows a) SED change as a function of fuel radial average enthalpy, and b) clad surface temperature increase as a function of fuel radial average enthalpy for the case with a burnup of 40 GWd/tU and 60 GWd/tU. The peak power is scaled by four times with a peak linear heat rate of 1697.4 kW/m. The results for the simulated RIA case NSRR VA-3 are also plotted for comparison. Notable in this figure is the high burnup fuel case result of SED versus enthalpy which is close to NSRR VA-3 with almost adiabatic power pulse, while lower burnup (40 GWd/tU) gives rise to lower SED due to an initial gap (8 micron) prior to the RIA. Up to 120 cal/g, the NSRR VA-3 case shows almost no cladding temperature increase, while the PWR cases have apparent higher cladding temperature increase and at ~80 cal/g, the cladding temperature escalation starts. Note that the DNB and film boiling were also predicted for the three NSRR cases, VA-3, VA-4, and RH-2, by Bison, however, the DNB in those cases is much delayed due to the narrow power pulse. Therefore, the cladding can have low ductility when the strong PCMI occurs in those test cases, but this does not seem to be the case with a wider power pulse. Note that the power pulse width would vary with the inserted reactivity, the higher the reactivity, the narrower is the power pulse width. The precise onset of DNB may vary depending on the power pulse width. The DNB, should it happen, could prevent the occurrence of the PCMI failure.

In the examination of the fresh fuel response shown in Figure 31, up to a very high power (x6), the DNB does not occur. Bison modeling without using any calibrated CHF correlations for the transient heat transfer has shown the apparent difference in the threshold to reach the DNB between the fresh fuel and irradiated fuel. The major difference could be caused by the relatively lower gap conductance and higher gap size of the fresh fuel; the edge-peaked radial power profile in irradiated fuel could have a higher heat flux from the fuel to cladding and coolant.

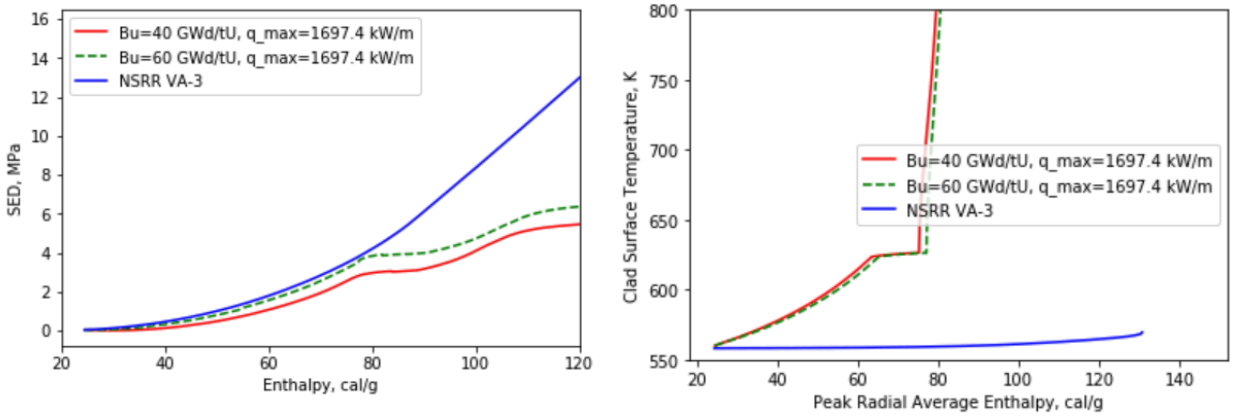


(a) SED (b) Clad surface temperature

Figure 30: Clad surface SED and temperature under the conditions with DNB using scaled power (peak power x 4)

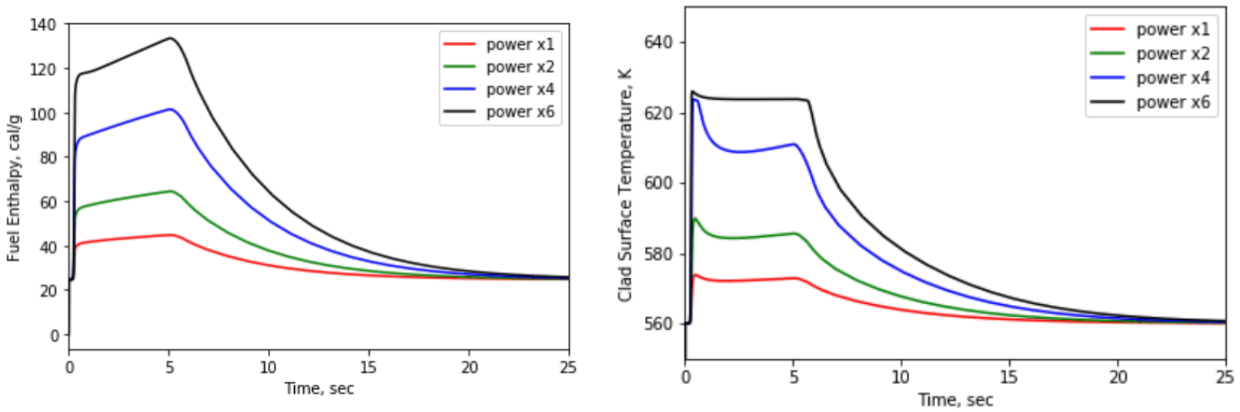


(a) Fuel enthalpy (b) Clad surface temperature

Figure 31: Comparison of fuel enthalpy and clad surface temperature for fresh fuel with different powers

The occurrence of DNB depends on the fuel rod condition, and the heat transfer in the fast transient could have a big impact on the response. Current investigation only models the CREA at zero power conditions, and DNB might be more limiting for the at-power conditions as suggested by current results. It is also possible, as suggested by current results, that the PCMI threshold may not be reached, while DNB can occur for RIAs in PWRs.

The existence of an oxide layer (for higher burnup fuel in particular) could also affect the fuel heat transfer, and CHF might be higher for the fast transient in RIA, also, depending on the duration of the high temperature, rewetting could occur so that the fuel could survive; those are not investigated in this report. It might be of interest to examine and quantify the effects of those variables on the DNB in the future study.

## 5.5 Fuel mechanical modeling

Elastic model is used for the modeling of the $UO_2$ pellet deformation in the current work. In a fast transient, the fuel can crack, and grain boundary separation can occur as a result of fission gas bubble expansion, and in some cases, fuel fragmentation can be observed. It might be of interest to examine the fuel response with a fuel mechanical model to account for those mechanisms. One fuel cracking

model, the smeared cracking model, which models the softening of the ceramic fuel after fracture, in the Bison fuel code, was tested for some cases with scaled power history. The results in Figure 32 have shown that the fuel surface displacement can differ and affect the SEDs as well. The impact of fuel mechanical modeling has not been thoroughly investigated, and a plastic deformation model might also be needed to quantify the impact on the calculated SED, since the plastic deformation of $UO_2$ may accommodate some interactions between the pellet and clad, which would reduce the clad deformation in the RIAs. The current result, however, shows that fuel mechanical models employed for the analysis could have appreciable impacts on the predictions.

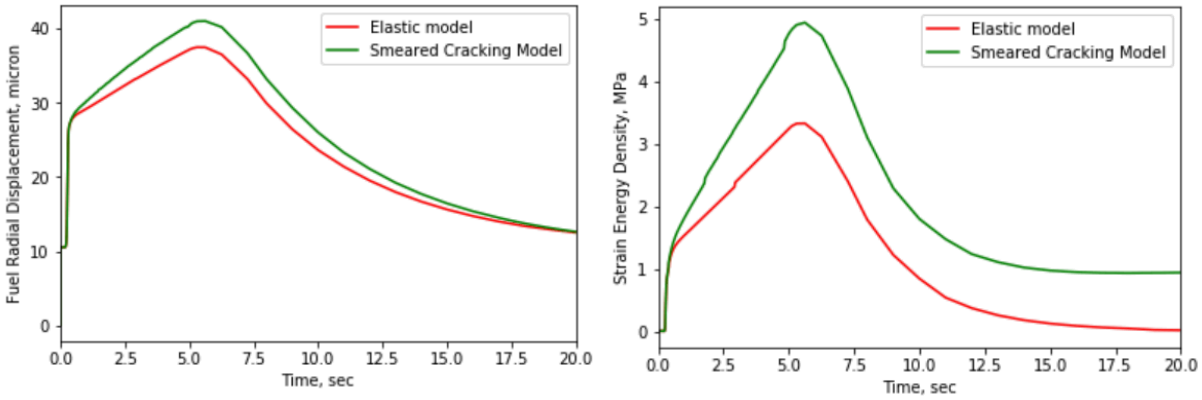


Figure 32: Comparison of fuel mechanical models on the fuel radial displacement and strain energy density in clad

## 6. CONCLUSIONS

This report summarizes the modeling of PWR fuel under RIA using Bison code. Full length PWR fuels with different initial burnups at 0, 20, 40, and 60 GWd/tU are modeled for CREA at HZP condition. Bison failure modeling method and a brief summary of validations on simulated RIA cases are also described. A benchmark case with a peripheral CREA in PWR with an inserted reactivity of $1.24 is selected as the baseline for the study. A simple scaling is applied to the rod average power during RIAs to extend the Bison modeling to different fuel enthalpies to quantify the margin to fuel failures.

Despite the concerns for the PCMI type of failures from CABRI and NSRR test facilities, the evaluation of REA using Bison code shows fuels with a wider power pulse in water reactor environment could have different responses than in the simulated RIA tests, and results indicate that a transition from PCMI to DNB could happen at relatively lower enthalpies: a better heat transfer from the fuel to coolant could increase cladding temperature and ductility, but at the same time also reduces the margin to DNB, which could cause high temperature oxidation and ballooning type of failures. The precise determination of the transition into DNB may rely on a more accurate input of the power histories in the simulated RIAs from core simulator, VERA. The limiting conditions in PWRs could be quite different than those tests with non-typical testing conditions, and the improvement of the modeling of thermal responses, such as, clad coolant heat transfer, gap heat transfer, clad thermal inertia, and radial power profiles could be important considerations of the RIAs for PWRs.

In the Bison application to the modeling of PWR fuel under RIA, results have shown that it is unlikely to have a PCMI type failure, and the failure enthalpy deduced from test reactor conditions could be conservative. DNB, an indicator of high temperature failure, appears to depend on the status of the fuel rod modelled, and results have shown that irradiated fuel could have lower threshold to DNB than the fresh fuel due to the difference in the fuel-clad gap heat transfer.

The work performed has demonstrated a successful application of Bison code in the modeling of RIAs for PWRs. Some aspects of the RIA modeling can be improved, and recommendations based on the current Bison modeling work are listed as follows.

- Computational efficiency of the Bison code still needs improvement; which has limited the application of many modeling capabilities developed in Bison code.
- Further validation of Bison's modeling in particular of the high temperature ballooning, and to identify the DNB threshold. NSRR TK series [4] and IGR/BIGR tests [16,17] with ballooning type failures are of interests to the Bison validation.
- The thermal response is still of interest to study, considering the large number of RIA tests not providing relevant data at such condition. Separative effects, such as the gap conductance, fuel-clad bonding, and fission gas release could affect the cladding temperature prediction. Those uncertainties need to be quantified.
- Some parameters, such as gap size, could have large impact on the RIA response, and material model selection could also affect the predicted failure metrics, and a further quantification of the uncertainties of those parameters are of interest to the future study.
- Modeling of RIAs with an appropriate fuel mechanical model to account for the expansion of fragmented fuel.

## REFERENCES


1. R. O. Montgomery, "Analysis of Reactivity Initiated Accident-Simulation Tests Conducted at the CABRI and NSRR Facilities in France and Japan," EPRI, Palo Alto, CA, 1002863, (2003).

2. T. Fuketa, F. Nagase, K. Ishijima, and T. Fujishiro. NSRR/RIA Experiments with High-burnup PWR Fuels. Nuclear Safety: Technical Progress Journal, 37(4):328–342, (1996).

3. T. Fuketa, et al., "NSRR/RIA Experiments with High-Burnup PWR Fuels," Proceedings of the 1997 ANS International Topical Meeting on Light Water Reactor Fuel Performance, Portland, USA, p669-676, March (1997).

4. T. Fuketa, et al., "Behavior of High-Burnup PWR Fuels with Low-tin Zircaloy-4 Cladding under Reactivity-Initiated-Accident Conditions," Nuclear Technology, Vol. 133, p50-62, Jan (2001).

5. J. Papin, M. Balourdet, F. Lemoine, F. Lamare, J. M. Frizonnet, and F. Schmitz. French Studies on High-burnup Fuel Transient Behavior under RIA Conditions. Nuclear Safety: Technical Progress Journal, 37(4):289–327, (1996).

6. H. Finnemann and A. Galati, "NEACRP-L-335: 3-D LWR Core Transient Benchmark Specification," NEACRP-L-335 (Revision 1), OECD NEA, (1992).

7. https://engineering.purdue.edu/PARCS/Code/TestSuite/CalculationMode/StandAloneMode/NEACRPPWR

8. C. P. Folsom, et. al., "RIA Experimentation Benchmark", (To be published in 2018).

9. W. Liu, N. Capps, A. Mai, and J. Rashid, "Development of a Failure Model for RIA Conditions," Consortium for Advanced Simulation of LWRs, CASL-L3_FMC_FUEL_P16_06, 2018.

10. S. K. Yagnik, A. Hermann, and R-C. Kuo, “Ductility of Zircaloy-4 Fuel Cladding and Guide Tubes at High Fluences,” Journal of ASTM International, Vol. 2, No. 5, p604 (2005).

11. F. Nagase and T. Fuketa, “Investigation of Hydride Rim Effect on Zircaloy-4 Cladding with Tube Burst Test,” Journal of Nuclear Science and Technology, Vol. 42, No. 1, p58-65 (2005).

12. Y. Fan and D.A. Koss, “The Influence of Multiaxial States of Stress on The Hydrogen Embrittlement of Zirconium Alloy Sheet,” Metallurgical Transactions A, Vol. 16, No. 4, p675-681, April (1985).

13. S. Leclercq, A. Parrot, and M. Leroy, “Failure Characteristics of Cladding Tubes under RIA Conditions,” Nuclear Engineering and Design, Vol. 238, No. 9, p2206-2218, September (2008).

14. J. Alvis, W. Liu, and K. Yueh, “Fuel Reliability Program: Proposed Reactivity Insertion Accident (RIA) Acceptance Criteria, Revision 1,” EPRI, 3002005540, (2015).

15. L. O. Jernkvist and A. R. Massih, “Nuclear Fuel Behavior under Reactivity Initiated Accident (RIA) Conditions,” OECD NEA, (2010).

16. L. Yegorova, K. Lioutov, and N. Jouravkova et al. Experimental Study of Narrow Pulse Effects on the Behavior of High Burnup Fuel Rods with Zr-1%Nb Cladding and UO2 Fuel (VVER Type) under Reactivity-Initiated Accident Conditions: Test Conditions and Results. Technical Report NUREG/IA-0213 Vol 1, IRSN/DPAM 2005-275, NSI RRC KI 3230, (2006).

17. L. Yegorova, K. Lioutov, and N. Jouravkova et al. Experimental Study of Narrow Pulse Effects on the Behavior of High Burnup Fuel Rods with Zr-1%Nb Cladding and UO2 Fuel (VVER Type) under Reactivity-Initiated Accident Conditions: Test Conditions and Results. Technical Report NUREG/IA-0213 Vol 2, IRSN/DPAM 2005-275, NSI RRC KI 3230, (2006).

18. V. Bessiron, "Modeling of Clad-to-coolant Heat Transfer for RIA Applications,” Journal of Nuclear Science and Technology, Vol. 44, No. 2, p. 211-221, (2007).

19. T. Sugiyama and T. Fuketa, “Effect of Cladding Surface Pre-oxidation on Rod Coolability under Reactivity Initiated Accident Conditions,” Journal of Nuclear Science and Technology, 41(11):1083–1090, (2004).

20. W. Liu and M. S. Kazimi, “Modeling Cladding-coolant Heat Transfer of High-burnup fuel during RIA,” ICONE14, Miami, Florida, (2006).

21. R. L. Williamson, G. Pastore, K. A. Gamble, R. J. Gardner, J. Tompkins, and W. Liu, "Development of a LOCA experimental benchmark for BISON," Consortium for Advanced Simulation of LWRs, CASL-U-2017-1422-000, (2017).

22. C. P. Folsom, R. L. Williamson, G. Pastore, and W. Liu, "Development of a RIA experimental benchmark for BISON," Consortium for Advanced Simulation of LWRs, CASL-U-2017-1403-000, (2017).

23. D. J. Diamond, B. P. Bromley, and A. L. Aronson, "Studies of the Rod Ejection Accident in a PWR," Technical Report W6382, Brookhaven National Laboratory, January 22, (2002).

24. J. Hales, et. al., "Bison Theory Manual," (2018).

25. A. Soba, A. Denis, L. Romero, E. Villarino, and F. Sardella, "A High Burnup Model Developed for the DIONISIO Code," Journal of Nuclear Materials, vol 433, p160-166, (2013).

26. Private communication with Dion Sunderland at Pacific Northwest National Laboratory, U.S.